PAPER

Origin of ^{17}O NMR chemical shifts based on molecular orbital theory: paramagnetic terms of the pre-α, α and β effects from orbital-to-orbital transitions, along with the effects from vinyl, carbonyl and carboxyl groups†

Keigo Matsuzaki, Satoko Hayashi [ID]* and Waro Nakanishi [ID]*

^{17}O NMR chemical shifts ($\delta(O)$) were analysed based on the molecular orbital (MO) theory, using the diamagnetic, paramagnetic and total absolute magnetic shielding tensors ($\sigma^d(O)$, $\sigma^p(O)$ and $\sigma^t(O)$, respectively). O^{2-} was selected as the standard for the analysis. An excellent relationship was observed between $\sigma^d(O)$ and the charges on O for O^{6+}, O^{4+}, O^{2+}, O^0 and O^{2-}. The data from H_2O, HO^+, HO^- and H_3O^+ were on the correlation line. However, such relationship was not observed for the oxygen species, other than above. The pre-α, α and β effects were evaluated bases on $\sigma^t(O)$, where the pre-α effect arises from the protonation to a lone pair orbital on O^{2-}, for an example. The 30−40 ppm and 20−40 ppm (downfield shifts) were predicted for the pre-α and β effects, respectively, whereas the values for the α effect was very small in magnitude, where the effect from the hydrogen bond formation should be considered. Similarly, the carbonyl effect in $H_2C{=}O$ and the carboxyl effects in $H(HO)C{=}O$ were evaluated from MeOH, together with $H_2C{=}CHOH$ from CH_3CH_2OH. Very large downfield shifts of 752, 425 and 207 ppm were predicted for $H_2C{=}O^*$, $H(HO)C{=}O^*$ and $H(HO^*)C{=}O$, respectively, together with the 81 ppm downfield shift for $H_2C{=}CHO^*H$. The origin of the effect were visualized based on the occupied-to-unoccupied orbital transitions. As a result, the origin of the ^{17}O NMR chemical shifts ($\delta(^{17}O)$) can be more easily imaged and understand through the image of the effects. The results would help to understand the role of O in the specific position of a compound in question and the mechanisms to arise the shift values also for the experimental scientists. The aim of this study is to establish the plain rules founded in theory for $\delta(^{17}O)$, containing the origin, which has been achieved through the treatments.

Introduction

NMR spectra are commonly measured and analysed on a daily basis to determine the structures and/or follow up the reactions. Indeed, ^1H and ^{13}C NMR spectroscopy is the most important tool for the purposes, but NMR spectra other than above are also measured on a daily basis.[1–4] NMR spectroscopy of ^{15}N, ^{17}O and ^{19}F atoms in the second period, has also been a very important technology in current chemical science research.[5–9] Among the nuclei, oxygen is the most abundant chemical element and it will form compounds with any other element, except for some atoms of the Group 18 element. It seems somewhat difficult to form compounds between them. Oxygen is also involved in the various biologically important species,

such as amino acids and nucleoacid bases,[10–16] together with the materials of high functionalities.[17,18] Measurements of ^{17}O NMR spectra in the natural abundance are now much easier by the advances in the spectrometer, irrespective of the very low natural abundance with the spin number of 5/2. As a result, lots of ^{17}O NMR chemical shifts ($\delta(O)$) of oxygen species have been reported thus far, of which values spread over 2500 ppm.

The importance of the NMR spectroscopy is widely recognized, as mentioned above. Experimental chemists usually analyse NMR spectra with the guidance of empirical rules.[1,2,9] The empirical rules are very useful for assigning the spectra, however, it is difficult to understand the origin of chemical shifts based on the rules. Indeed, only the chemical shift of the reference species is usually provided in such NMR analysis, but any concept and/or data, that help us to image the origin of the chemical shifts, are not provided. As a result, it is very difficult to visualize the origin of the NMR chemical shifts, especially for experimental scientists, who are not the specialists in this field, including the authors. (They are originally experimental chemists, who use calculations extensively to confirm the

Faculty of Systems Engineering, Wakayama University, 930 Sakaedani, Wakayama 640-8510, Japan. E-mail: hayashi3@wakayama-u.ac.jp; nakanisi@wakayama-u.ac.jp
† Electronic supplementary information (ESI) available: Additional tables and figures and the fully optimized structures given by Cartesian coordinates, together with total energies. See DOI: https://doi.org/10.1039/d4ra00843j
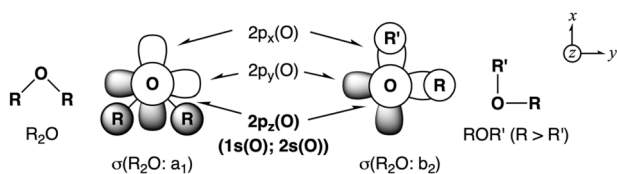
causality in the experimental results.) This must be the extreme contrast to the cases of the electronic spectra and the infrared spectra, for example. It is easily come to mind the image of the origin for the spectra. They correspond to the electronic transitions between the occupied and unoccupied energy levels and the transitions between the energy levels of internal vibrations, respectively, in molecules and/or atoms.

Our research interested, therefore the aim of this study, is to establish the plain rules founded in theory for the origin of the ^{17}O NMR chemical shifts for the better understanding of the phenomena. The origin should be visualized based on the specific concepts, such as molecular orbitals (MOs). The plain rules with the origin should be easily imaged and understood by the experimental scientists who are not the specialists. This purpose is given more importance, in this work, than the usual calculations of the NMR parameters, reproducing the observed values accurately and/or to predict well the shift values of unknown target compounds. The results should help to understand the role of O in the specific position of a compound in question and the mechanisms to arise the shift values.

Scheme 1 shows the axes in ROR, used for the analysis, together with some MOs and/or AOs (atomic orbitals). The direction of the p-type lone pair orbital ($n_p(O)$) in the symmetric ROR was set to the z-axis, which was perpendicular to the molecular plane, the bisected $\angle C_R O C_R$ direction is set to the x-axis, and that perpendicular to the two is set to the y-axis. In the case of unsymmetric ROR′ (R > R′), the z-axis is set to the direction of $n_p(O)$, while the y- and x-axes are set appropriately in the plane of O–C_R and O–$C_{R'}$. The axes for the species other than above are shown in the individual figures.

The α, β, γ and δ effects are well known as the experimental rules, which correspond to the methyl substitutions in the processes of –O–H → –O–CH$_3$, –O–CH$_3$ → –O–CH$_2$–CH$_3$, –O–CH$_2$–CH$_3$ → –O–CH$_2$–CH$_2$–CH$_3$ and –O–CH$_2$–CH$_2$–CH$_3$ → –O–CH$_2$–CH$_2$–CH$_2$–CH$_3$, respectively. The α, β and γ effects in the ^{17}O NMR chemical shifts are typically found at −40 ppm (upfield shifts), +30 ppm (downfield shifts), −6 ppm (upfield shifts), respectively, with the δ effect being negligibly small, based on the observed values. The α, β and γ effects are analysed based on the MO theory. We have proposed the "pre-α effect" to establish the plain rules and understand the mechanisms in a unified form.[19] The "pre-α effect" is defined to originate from the protonation to a lone pair orbital of O (O^{2-} → OH^-, for example). The pre-α, α, β and γ effects are discussed for $\delta(^{17}O)$ in R–^{17}O–R′, where R and R′ are the saturated hydrocarbons. The values for the effects are calculated per unit group (per Me or H). The effects on $\delta(^{17}O)$ in the unsaturated moieties are also be discussed, exemplified by the vinyl, carbonyl and carboxyl groups, in this paper. The plain rules, established based on the theory, need to be as simple and easily understood.

The chemical shifts of the respective structures can be theoretically calculated. The origin will be elucidated based on the MO theory. The total absolute magnetic shielding tensors (σ^t) are used for the analysis, since σ^t can be calculated with satisfactory accuracy. As shown in eqn (1), σ^t is decomposed into the diamagnetic and paramagnetic shielding tensors (σ^d and σ^p, respectively).[20–22] The magnetic shielding tensors consist of three components: σ_{xx}^m, σ_{yy}^m and σ_{zz}^m (m = d, p and t). Eqn (2) shows the relationship. As shown in eqn (3), σ^d is simply expressed as the sum of the contributions over the occupied orbitals (ψ_i, so is ψ_j), where the contribution from each ψ_i to σ^d (σ_i^d) is proportional to the average inverse distance of electrons from nuclei in ψ_i, $<r_i^{-1}>$ (eqn (4)).[23] σ^p is evaluated by the Coupled-Hartree-Fock (CPHF) method. σ^p can be decomposed into the contributions from the occupied orbitals or the orbital-to-orbital transitions,[24] under the DFT levels. σ^p is shown in eqn (5), where the contributions from the occupied-to-occupied orbital transitions are neglected.[19,23] The process to evaluate σ^p is highly complex, therefore, σ^p will be discussed based on the approximate image derived from eqn (6),[24] where $(\varepsilon_a - \varepsilon_i)^{-1}$ is the reciprocal orbital energy gap, ψ_k is the k-th orbital function, $\hat{L}_{z,N}$ is orbital angular momentum around the resonance nucleus N, and r_N is the distance from N.

$$\sigma^t = \sigma^d + \sigma^p \tag{1}$$

$$\sigma^m = (\sigma_{xx}^m + \sigma_{yy}^m + \sigma_{zz}^m)/3 \ (m = \text{d, p and t}) \tag{2}$$

$$\sigma^d = \sum_i^{occ} \sigma_i^d \tag{3}$$

$$\sigma_i^d = (\mu_o e^2 / 12\pi m_e)\langle r_i^{-1} \rangle \tag{4}$$

$$\sigma^p = \sum_i^{occ} \sigma_i^p = \sum_i^{occ} \sum_a^{unocc} \sigma_{i \to a}^p \tag{5}$$

$$\sigma_{zz}^p = -(\mu_o e^2 / 2m_e^2) \sum_i^{occ} \sum_a^{unocc} (\varepsilon_a - \varepsilon_i)^{-1} \cdot \left\{ \left\langle \psi_i | \hat{L}_z | \psi_a \right\rangle \right.$$
$$\left. \times \left\langle \psi_a | \hat{L}_{z,N} r_N^{-3} | \psi_i \right\rangle + \left\langle \psi_i | \hat{L}_{z,N} r_N^{-3} | \psi_a \right\rangle \left\langle \psi_a | \hat{L}_z | \psi_i \right\rangle \right\} \tag{6}$$

The NMR chemical shifts of the atoms in the higher periods are predominantly controlled by the σ^p term. The origin and the mechanisms have been thoroughly analysed, such as for $\delta(Se)$.[19] Contrary to the atoms in the higher period, the NMR chemical shifts of the atoms in the second period are controlled by both the σ^d and σ^p terms. Therefore, the mechanisms such as for $\delta(O)$ will be more complex. Here, we discuss the origin and mechanisms for $\delta(O)$ based on the MO theory, employing the pre-α, α and β effects, together with the effects from the vinyl, carbonyl and carboxyl groups. Our explanation is intended to clarify the shift values, mainly based on the orbital-to-orbital ($\psi_i \to \psi_a$)

Scheme 1 Axes in ROR and ROR′, analysed in this work, along with some orbitals. The atomic orbitals (AOs) of 1s (O) and 2s (O) are not drawn, since they overlap 2p$_z$ (O), if illustrated.

transitions, as aforementioned. The earlier investigations on δ(Se) will help to understand δ(O) easier, we believe, due to the similarities in the basic structures of the species consisted of the atoms.[19]

Methodological details in calculations

Calculations were performed using the Gaussian 09 program package, including GaussView.[25] The structures were optimized for various oxygen species with the 6–311++G(3df,3pd) (6D10F) basis set (BSS-A). The structural optimizations were performed at the DFT[26–29] (L1) and/or MP2 [30–32] (L2) levels (L = L1 + L2), after some pre-optimizations. The gauge-independent atomic orbital (GIAO) method[33–37] was applied to calculate the absolute magnetic shielding tensors of O [σ(O)]. To examine the level dependence on the σ(O), the σ(O) values were calculated at the various L1 levels of B3LYP,[26–29] CAM-B3LYP,[38] PBE,[39] PBE0,[40] LC-ωPBE[41] and ωB97X-D[42] with BSS-A (L1/BSS-A) and the L2 level. The basis set of def2TZVP[43,44] was also applied at the B3LYP level (B3LYP/def2TZVP). The solvent effect of CHCl$_3$ was evaluated with the polarizable continuum model (PCM),[45] if necessary. The 6-311+G(3d,3p) (6D10F) basis set (BSS-B) operates similarly well to BSS-A, but the results are not discussed.

A utility program[46] was applied to evaluate the contributions from each ψ_i and/or $\psi_i \rightarrow \psi_a$ transition. The procedure is explained in Appendix of the ESI.† The charge on O (Q(O)) was obtained with the natural population analysis (NPA).[47]

Results and discussion

Search for suitable level in the calculations: setting the standard for the calculated σ^t(O) values *versus* the observed δ(O) values

We will tentatively use σ^t(O: S) and δ(O: S) as the calculated and observed values, respectively, in this paper, to avoid confusing the discussion, although this notation might not be completely theoretically appropriate. In this case, σ^t(O: S) and δ(O: S), respectively, stand for the shift values of oxygen species, S.

Before detailed discussion to determine the suitable calculation level in this work, it is necessary to set up the appropriate standard for σ^t(O: S). The δ(O: H$_2$O) value is taken as the standard for δ(O: S). Therefore, it seems good idea, at first glance, that the σ^t(O: H$_2$O) value is also taken as the standard for σ^t(O: S), when the σ^t(O: S) values are compared directly with the δ(O: S) values. However, this choice will not give good results, since the observed and calculated conditions are very different especially for H$_2$O. Water forms poly-clusters through hydrogen bonds (HBs) in liquid,[48] but a single molecule in the gas phase is assumed in the calculation conditions.

To avoid large differences in the chemical shifts, due to the differences between the observed and calculated conditions in water, we selected the δ(O: Me$_2$O) value of −52.50 ppm for the common standard of δ(O: S) and σ^t(O: S). Namely, δ(O: Me$_2$O) = σ^t(O: Me$_2$O) = −52.50 ppm is chosen at the common standard for both, where σ^t(O: Me$_2$O) should be denoted by $\Delta\sigma^t$(O: Me$_2$O), so σ^t(O: S) is by $\Delta\sigma^t$(O: S). The treatment leads $\Delta\sigma^t$(O: H$_2$O) = 0.00 ppm, fictionally. However, the sign of $\Delta\sigma^t$(O: S) is basically

just the opposite to that of δ(O: S). Therefore, $-\Delta\sigma^t$(O: S) should be used, instead of $\Delta\sigma^t$(O: S), for the direct comparison between the calculated and observed values, where δ(O: Me$_2$O) = −52.50 ppm is used as the common standard of both observed and calculated values.

It is now possible to search for the suitable level in this work, after setting up the initial research conditions. The σ^t(O: S) values for various oxygen species S (ROR + ROR′) were calculated at the DFT levels of B3LYP,[26–29] CAM-B3LYP,[38] PBE,[39] PBE0,[40] LC-ωPBE[41] and ωB97X-D[42] (L1) with BSS-A (L1/BSS-A// L1/BSS-A), together with σ^d(O: S) and σ^p(O: S). The MP2 level (L2) is also applied for the calculations. However, only σ^t(O: S) were obtained at the MP2 level (MP2/BSS-A//MP2/BSS-A). The results are collected in Tables S1–S8 of the ESI.† The calculated values are very close with each other.

The $-\Delta\sigma^t$(O: S) values calculated at the L (=L1 + L2) levels are plotted *versus* the corresponding δ(O: S), respectively. Fig. 1 shows the plots for S of (ROR + ROR′: the 31 species) at B3LYP. The plot is analysed assuming the linear relationship ($y = ax + b$: R_c^2 (the square of the correlation coefficient)), where (a, b, R_c^2) = (0.936, 2.88, 0.982) for the plot in Fig. 1. Similar calculations were performed at various L. Table 1 collects the correlations. Judging from the (a, b, R_c^2) values in Table 1, B3LYP, CAM-B3LYP and PBE levels seem suitable for our purpose together with others, the b value seems somewhat larger at PBE, and the a values are less than 0.90 at PBE0, LC-ωPBE and ωB97X-D. The MP2 level gave similar results but R_c^2 = 0.934, the poorest value in Table 1. The a value amounts to 0.960 at B3LYP, if the solvent effect of CHCl$_3$ is considered. The results with B3LYP/def2TZVP are shown in entry 9 of Table 1. The a and b values seem very good, whereas R_c^2 = 0.926. The differences between observed and calculated values are around 20 ppm in magnitudes for *s*-BuOMe and *s*-BuOEt. The B3LYP/BSS-A method is selected for
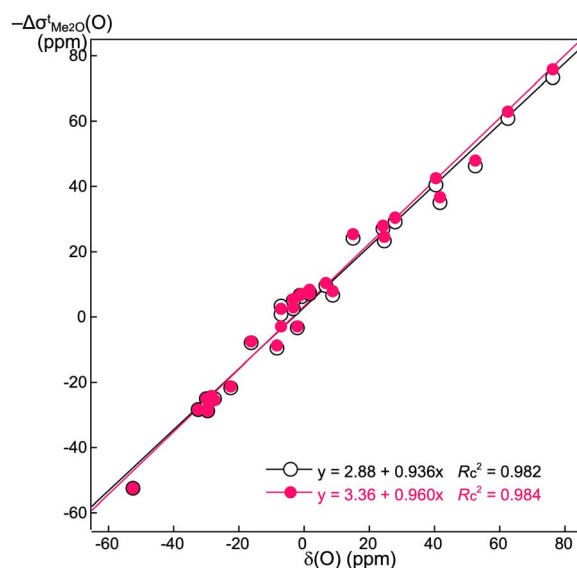

Fig. 1 Plots of the calculated $-\Delta\sigma^t$(O: S) *versus* the observed δ(O: S) (S: ROR + ROR′) at the B3LYP level, with (●) and without (○) the solvent effect of CHCl$_3$.

Table 1 Correlations in the plots of calculated $-\Delta\sigma^t$(O: S) versus observed δ(O: S) for the ether type oxygen species, S (ROR + ROR′)[a,b]

Entry	Level (L)	a	b	R_c^2	N
1	B3LYP	0.936	2.88	0.982	31
2	CAM-B3LYP	0.911	2.30	0.979	31
3	PBE	0.976	5.43	0.982	31
4	PBE0	0.894	1.55	0.978	31
5	LC-ωPBE	0.845	−2.09	0.979	31
6	ωB97X-D	0.886	−0.07	0.982	31
7	MP2	0.933	1.24	0.934	31
8[c]	B3LYP	0.960	3.36	0.984	31
9[d]	B3LYP	0.929	1.22	0.926	31

[a] Calculated with the GIAO method under L/BSS-A. [b] Observed data are used for the corresponding species in the plot. [c] Under the solvent effect of CHCl$_3$. [d] Calculated with B3LYP/def2TZVP.

the calculations based on the results. Our aim of this work can be achieved even without the solvent effect in the calculations. The level is most popularly accepted also by the experimental researchers, which is significant for our purposes. Not so different results will be obtained when other levels in Table 1 are applied to the calculations.

Analysis of ^{17}O NMR chemical shifts and the standard species

To determine the suitable standard for the analysis of ^{17}O NMR chemical shifts based on σ^d(O), σ^p(O) and σ^t(O), the values were calculated for O[6+], O[4+], O[2+], O[0] and O[2−] with B3LYP/BSS-A and MP2/BSS-A. Table 2 summarizes the results. The σ^t(O) values for O[6+], O[4+] and O[2−], calculated with the two methods, were very close to each other. O[2−] was selected as the standard among the three, after the case of σ^p(Se).[19] It is very favourable to use σ^p(O: O[2−]) = 0.0 ppm as a standard, especially for our purpose, although σ^p(O: O[4+]) and σ^p(O: O[6+]) are also 0.0 ppm. The electronic [1]S$_o$ state of O[2−] with eight valence electrons by the octet rule and its spherical electron distribution are also favourable for the purpose.

Table 3 collects the σ^d(O), σ^p(O), σ^t(O), $\Delta\sigma^d$(O), $\Delta\sigma^p$(O) (=σ^p(O) (since σ^p(O): O[2−] = 0 ppm)) and $\Delta\sigma^t$(O) values for various oxygen species of **1–36**, calculated with B3LYP/BSS-A, together with the Q(O) values with NPA. The $\Delta\sigma^*$(O: S) (* = d, p and t) values are calculated from O[2−], according to $\Delta\sigma^*$(O: S) = σ^*(O: S) − σ^*(O: O[2−]). The extended conformers are selected for the calculations, since they are less three-dimensionally crowded than others, although others would contribute in some cases (Table S9 of the ESI†).

Scheme 2 explains the method to calculate the effects, exemplified by the pre-α, α and β effects. The effects are calculated as $\Delta\sigma^t$(O: S)$_e$ = (1/n)[σ^t(O: S) − σ^t(O: S$_e$)], where S$_e$ are the starting species to give the effects and n is the factor to make $\Delta\sigma^*$(O: S)$_e$ per unit group. In the case of the β effect from Me$_2$O to Et$_2$O, Et$_2$O, Me$_2$O and 2 correspond to S, S$_e$ and n, respectively, in the equation. The difference of $\Delta\sigma^t$(O: S) between S = Et$_2$O (σ^t(O) = 261 ppm) and Me$_2$O (σ^t(O) = 323 ppm) is −62 ppm, which correspond to the 2β effect (=$\Delta\sigma^t$(O: S) = σ^t(O: S) − σ^t(O: O[2−])). The $\Delta\sigma^*$(O: S) values are abbreviated by Δ in Scheme 2. Therefore, the β effect in this process is evaluated to be 31 ppm (=Δ/2), for example. The $\Delta\sigma^d$(O: S)$_e$ and $\Delta\sigma^p$(O: S)$_e$ values for the effect are calculated similarly.

The pre-α, α, β, γ and δ effects are calculated, according to the method, so are the vinyl, carbonyl and carboxyl effects. The pre-α, α, β, γ and δ effects are calculated for R-O-R′ (R, R′: saturated hydrocarbons), while the unsaturated moieties of the vinyl, carbonyl and carboxyl effects are calculated from EtOH, MeOH and MeOH, respectively. Table 3 collects the values. Scheme 3 visualizes the effects with the values.

Behaviour of σ^d(O)

The behaviour of the calculated σ^d(O) values can be understood by considering the two factors derived from eqn (3) and (4). If the number of occupied AOs on O increases, the σ^d(O) values become larger, whereas the magnitude of each σ_i^d(O: AO) becomes smaller, especially that for the outer AOs. The average distance of the electrons from the nucleus O (r_i) in each AO becomes larger due to the increase in electron–electron repulsion if the number of occupied AOs increases. In this case, each $< r_i^{-1}>$ (and therefore σ_i^d(O)) in eqn (4) decrease. The σ_i^d(O) values in Table 3 are well understood as the total effect of the two.

To examine the effect of the charge on O (Q(O)), the σ^d(O) values are plotted versus Q(O) for O[6+], O[4+], O[2+], O[0] and O[2−] (**1**), as shown in Fig. 2; an excellent correlation by a quadratic function was obtained ($y = -1.673x^2 - 10.24x + 394.5$: $R_c^2 = 1.000$). The results show that the σ^d(O) values are excellently correlated to Q(O) if the oxygen species has no ligands. The σ^d(O) values for H$_2$O (**7**), HO[+] (**30**), HO[−] (**2**) and H$_3$O[+] (**25**) are also plotted versus Q(O) (see Table 3 for the data). The data points appear on or slightly below the regression curve. The data for HO[+] (**30**) and H$_3$O[+] (**25**) are basically located on the regression curve, and those for H$_2$O (**7**) and HO[−] (**2**) are located slightly below the curve. The results show that the H atom(s) on O affect somewhat on σ^d(O), in addition to the effect on Q(O),

Table 2 Absolute shielding tensors for [17]O* (* = 6+, 4+, 2+, 0 and 2−) in the singlet state[a]

Nuclear	Configuration	σ_{B3LYP}^d(O: 1s)	σ_{B3LYP}^d(O: 2s)	σ_{B3LYP}^d(O: 2p)	σ_{B3LYP}^d(O)	σ_{B3LYP}^p(O)	σ_{B3LYP}^t(O)	σ_{MP2}^t(O)
O[6+]	(2s)[0](2p)[0]	272.70	0.00	0.00	272.70	0.00	272.70	272.82
O[4+]	(2s)[2](2p)[0]	271.45	55.54	0.00	327.00	0.00	327.00	327.09
O[2+]	(2s)[2](2p)[2]	270.87	49.87	46.41 (×1)	367.15	8382.15	8749.31	6551.47
O[0]	(2s)[2](2p)[4]	270.67	45.42	39.18 (×2)	394.45	6794.55	7189.01	6010.58
O[2−]	(2s)[2](2p)[6]	270.66	43.73	31.31 (×3)	408.33	0.00	408.33	407.67

[a] Calculated by applying the GIAO method under B3LYP/BSS-A and MP2/BSS-A.

Table 3 The $\sigma^d(O)$, $\sigma^p(O)$, $\sigma^t(O)$, $\Delta\sigma^d(O)_e$, $\Delta\sigma^p(O)_e$ and $\Delta\sigma^t(O)_e$ values for various oxygen species, **1–36**, along with the pre-α, α, β, γ and δ effect and the effects from the vinyl, carbonyl and carboxyl groups, based on $\Delta\sigma^t(O)_e^{a,b}$

Species (sym)	$Q(O)$	$\sigma^d(O)$	$(\Delta\sigma^d(O))$	$\sigma^p(O)^c$	$\sigma^t(O)$	$(\Delta\sigma^t(O))$	$\Delta\sigma^d(O)_e^d$	$\Delta\sigma^p(O)_e^d$	$\Delta\sigma^t(O)_e^d$	Effect
O^{2-} (**1**: O_h)	−2.000	408.33	(0.00)	0.00	408.33	(0.00)	0.00	0.00	0.00	—
OH^- (**2**: $C_{\infty v}$)	−1.372	396.59	(−11.74)	−19.56	377.03	(−31.29)	−11.74	−19.56	−31.29	Pre-α
MeO^- (**3**: C_{3v})	−0.976	415.05	(6.72)	−133.83	281.22	(−127.11)	18.46	−114.27	−95.81	α
EtO^- (**4**: C_s)	−0.938	419.47	(11.15)	−290.56	128.91	(−279.41)	4.42	−156.73	−152.31	β
$i\text{-}PrO^-$ (**5**: C_s)	−0.942	423.43	(15.11)	−297.32	126.12	(−282.21)	4.19	−81.75	−77.55	β
$t\text{-}BuO^-$ (**6**: C_s)	−0.970	427.54	(19.22)	−227.30	200.24	(−208.08)	4.17	−31.16	−26.99	β
H_2O (**7**: C_{2v})	−0.929	392.85	(−15.47)	−66.72	326.13	(−82.19)	−7.74	−33.36	−41.10	Pre-α
$MeOH$ (**8**: C_s)	−0.740	395.07	(−13.26)	−72.87	322.20	(−86.13)	2.21	−6.15	−3.94	α
$EtOH$ (**9**: C_s)	−0.751	398.40	(−9.93)	−108.33	290.07	(−118.25)	3.33	−35.46	−32.13	β
$i\text{-}PrOH$ (**10**: C_1)	−0.752	402.81	(−5.52)	−152.24	250.57	(−157.75)	3.87	−39.68	−35.81	β
$t\text{-}BuOH$ (**11**: C_s)	−0.759	406.99	(−1.34)	−180.47	226.52	(−181.81)	3.97	−35.87	−31.89	β
$n\text{-}PrOH$ (**12**: C_s)	−0.747	401.99	(−6.33)	−110.17	291.82	(−116.51)	3.59	−1.85	1.74	γ
$n\text{-}BuOH$ (**13**: C_s)	−0.747	405.29	(−3.03)	−112.68	292.62	(−115.71)	3.30	−2.50	0.80	δ
Me_2O (**14**: C_{2v})	−0.599	396.12	(−12.21)	−73.37	322.75	(−85.58)	1.63	−3.32	−1.69	α
$EtOMe$ (**15**: C_s)	−0.604	397.46	(−10.86)	−105.43	292.04	(−116.29)	1.35	−32.06	−30.71	β
$i\text{-}PrOMe$ (**16**: C_1)	−0.614	401.79	(−6.53)	−128.26	273.53	(−134.79)	2.84	−27.45	−24.61	β
$t\text{-}BuOMe$ (**17**: C_s)	−0.622	405.31	(−3.01)	−141.91	263.41	(−144.92)	3.07	−22.85	−19.78	β
$n\text{-}PrOMe$ (**18**: C_s)	−0.603	400.83	(−7.49)	−105.99	294.84	(−113.48)	3.37	−0.57	2.80	γ
$n\text{-}BuOMe$ (**19**: C_s)	−0.600	405.13	(−3.20)	−110.00	295.13	(−113.19)	4.30	−4.00	0.29	δ
Et_2O (**20**: C_{2v})	−0.618	396.85	(−11.47)	−136.13	260.72	(−147.60)	0.37	−31.38	−31.01	β
$i\text{-}Pr_2O$ (**21**: C_2)	−0.631	401.23	(−7.10)	−177.41	223.82	(−184.50)	−1.95	−33.70	−35.65	β
$t\text{-}Bu_2O$ (**22**: C_2)	−0.656	393.82	(−14.50)	−196.90	196.92	(−211.41)	−3.77	−28.97	−32.74	β
$n\text{-}Pr_2O$ (**23**: C_{2v})	−0.610	397.47	(−10.86)	−132.00	265.47	(−142.86)	0.31	2.07	2.37	γ
$n\text{-}Bu_2O$ (**24**: C_{2v})	−0.609	407.03	(−1.29)	−140.01	267.02	(−141.30)	4.78	−4.01	0.78	δ
H_3O^+ (**25**: C_{3v})	−0.748	397.19	(−11.13)	−93.28	303.92	(−104.41)	−3.71	−31.09	−34.80	Pre-α
MeH_2O^+ (**26**: C_s)	−0.624	400.40	(−7.93)	−94.92	305.48	(−102.85)	3.21	−1.64	1.56	α
EtH_2O^+ (**27**: C_1)	−0.646	408.30	(−0.02)	−132.51	275.80	(−132.53)	7.90	−37.59	−29.68	β
Me_3O^+ (**28**: C_{3v})	−0.407	403.21	(−5.12)	−106.15	297.05	(−111.27)	2.01	−4.29	−2.29	α
Et_3O^+ (**29**: C_3)	−0.457	397.04	(−11.29)	−158.79	238.24	(−170.08)	−2.06	−17.55	−19.60	β
OH^+ (**30**: $C_{\infty v}$)	0.480	386.73	(−21.60)	1138.35	1525.08	(1116.76)	−21.60	1138.35	1116.76	Pre-α
$H_2C{=}CHOH$ (**31**: C_s)	−0.695	402.75	(−5.58)	−193.80	208.95	(−199.38)	4.35^e	$−85.47^e$	$−81.12^e$	C=C
$H_2C{=}CHOMe$ (**32**: C_s)	−0.561	402.34	(−5.99)	−173.97	228.36	(−179.96)	$−0.41^f$	19.83^f	19.42^f	C=C
$PhOH$ (**33**: C_s)	−0.700	391.76	(−16.57)	−183.66	208.10	(−200.23)	$−3.31^g$	$−110.79^g$	$−114.10^g$	C_6H_5
$H_2C{=}O$ (**34**: C_{2v})	−0.499	404.50	(−3.82)	−833.77	−429.27	(−837.59)	9.44^g	$−760.90^g$	$−751.46^g$	C=O
$H(HO)C{=}O^*$ (**35**: C_s)	−0.582	404.48	(−3.84)	−506.77	−102.29	(−510.62)	9.42^g	$−433.90^g$	$−424.48^g$	OC=O*
$H(HO^*)C{=}O$ (**36**: C_s)	−0.687	399.82	(−8.51)	−284.37	115.44	(−292.88)	4.75^g	$−211.50^g$	$−206.75^g$	*OC=O

^{a} Calculated with the GIAO method under B3LYP/BSS-A. ^{b} $\Delta\sigma^*(O:S) = \sigma^*(O:S) - \sigma^*(O:O^{2-})$ (* = d, p and t). ^{c} $\Delta\sigma^p(O) = \sigma^p(O)$, since $(\sigma^p(O:O^{2-}) = 0$ ppm). ^{d} $\Delta\sigma^*(O:S)_e = (1/n)(\Delta\sigma^*(O:S) - \Delta\sigma^*(O:S_e))$, see text for n, S and S_e. ^{e} From EtOH. ^{f} From $H_2C{=}CHOH$. ^{g} From MeOH.
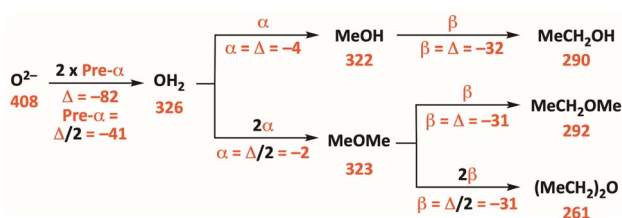
Scheme 2 Evaluation of the pre-α, α and β effects. The $\sigma^t(O:S)$ values in ppm are given in red bold and the differences between the two are by Δ.

although the $Q(O)$ value may change depending on the calculation method.

Analysis of $\delta(O)$ based on the MO theory

The behaviour of $\sigma^d(O:S)$, where S has at least one alkyl group, is examined, next. Fig. 3 shows the plot of $\sigma^d(O:S)$ versus $Q(O)$ for **1–36**, other than those in Fig. 2. The $\sigma^d(O:S)$ values are analysed separately by the types of S: RO^- (**3–6**), ROH (**8–13**), ROMe (**14–19**) and ROR (**20–24**), RH_2O^+ (**26** and **27**), and R_3O^+ (**28** and **29**), along with others (**31–36**). Each plot for a type of S appears almost the y-direction, except for S of **31–36**. The ranges of $\sigma^d(O)$ amount to 15 ppm, while those of $Q(O)$ are very small in each group. The $\sigma^d(O:S)$ values become larger in the order of R = Me < Et < i-Pr < t-Bu for RO^-, ROH and ROMe. The structural dependence appears to control the $\sigma^d(O:S)$ values.

As mentioned above, the magnitudes of $\Delta\sigma^d(O:S)$ are less than 15 ppm for most species in each group of species (see Table 3). However, the magnitudes of $\Delta\sigma^d(O:S)$ are larger than 15 ppm for i-PrO⁻ (**5**: $\Delta\sigma^d(O)$ = 15.1 ppm), t-BuO⁻ (**6**: 19.2 ppm), H_2O (**7**: −15.5 ppm), OH^+ (**30**: −21.6 ppm) and PhOH (**33**: −16.6 ppm). The first two are the RO^- type, and the last three are H_2O, OH^+ and PhOH. The results for OH^+ are effectively understood based on $Q(O)$, where the larger magnitude in $\Delta\sigma^d(O:S)$ for OH^+ (**30**) potentially comes from the larger positive $Q(O)$ value (=0.482). The magnitudes of $\Delta\sigma^d(O:S)$ are much smaller than
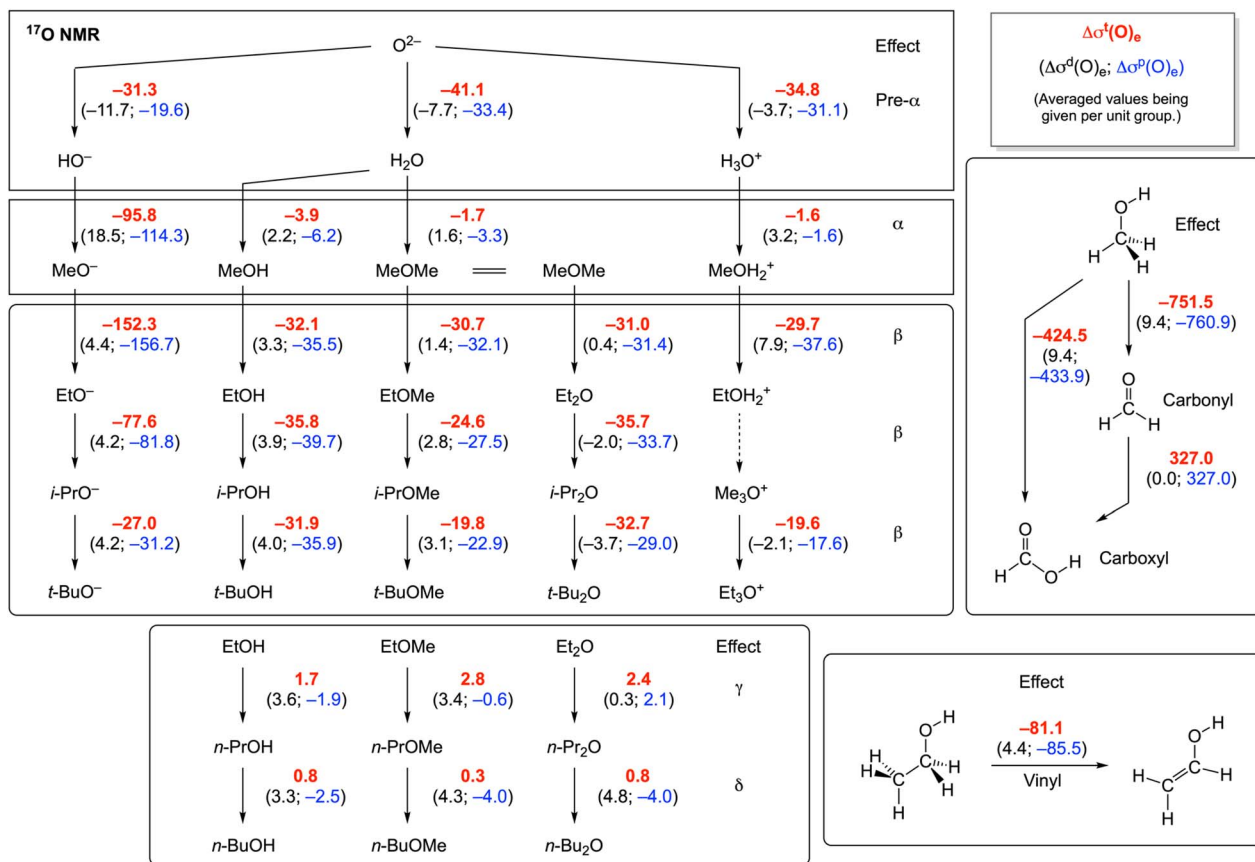
Scheme 3 Pre-α, α, β, γ and δ effects, along with the effects from the vinyl, carbonyl and carboxyl groups, on the ^{17}O NMR chemical shifts, calculated with the GIAO method under B3LYP/BSS-A.
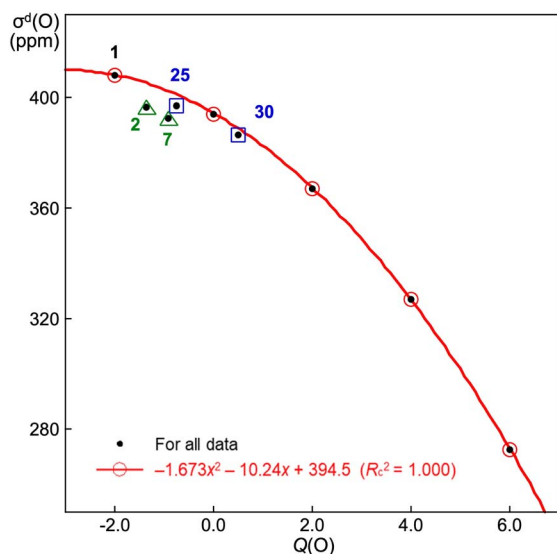

Fig. 2 Plot of $\sigma^d(O)$ versus $Q(O)$ for O^{6+}, O^{4+}, O^{2+}, O^0 and O^{2-} (**1**), together with H_2O (**7**), HO^+ (**30**), HO^- (**2**) and H_3O^+ (**25**).
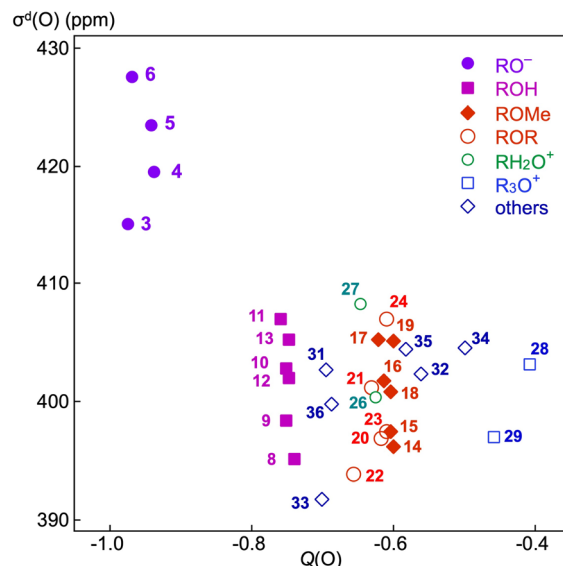

Fig. 3 Plots of $\sigma^d(O)$ versus $Q(O)$ for various oxygen species **1–36**, other than those in Fig. 2.

those of $\Delta\sigma^p(O: S)$. The contributions from $\Delta\sigma^d(O: S)$ to $\Delta\sigma^t(O: S)$ are less than 10%, except for OH^- (**2**: 37.5%), H_2O (**7**: 18.8%), MeOH (**8**: 15.4%), Me_2O (**14**: 14.3%) and H_3O^+ (**25**: 10.7%). Specifically, $\Delta\sigma^p(O: S)$ contributes predominantly to $\Delta\sigma^t(O: S)$,

relative to the case of $\Delta\sigma^d(O: S)$. As a result, ^{17}O NMR chemical shifts can be analysed mainly by $\Delta\sigma^p(O: S)$; however, $\Delta\sigma^d(O: S)$ should be considered when necessary.

Effect of hydrogen bonds on ^{17}O NMR chemical shifts

What is the effect from the hydrogen bonds (HBs) on $\sigma^d(O)$, $\sigma^p(O)$ and $\sigma^t(O)$? The effect is to be clarified before the detailed discussion of the values. The $\sigma^d(O)$, $\sigma^p(O)$ and $\sigma^t(O)$ values for the various ether monomers (ROR + ROR′), calculated with B3LYP/BSS-A, are collected in Table S1 of the ESI† (see also Fig. 1). The $\sigma^t(O)$ value of the Me_2O dimer is calculated to be only 1.4 ppm downfield of that of the monomer, therefore, the effect of the dimer formation in ROR + ROR′ on $\delta(O)$ is considered to be negligible. Namely, the data of the monomers can be used for those of ROR + ROR′.

The $\sigma^t(O)$ values are calculated for the monomers and the dimers of ROH and RCOOH, together with the differences in $\sigma^t(O)$ between the dimers and the monomers $\Delta\sigma^t(O)_{dm}$ [$=\sigma^t(O\text{: dimer}) - \sigma^t(O\text{: monomer})$]. The solvent effect of $CHCl_3$ on the $\sigma^t(O)$ and $\Delta\sigma^t(O)_{dm}$ values are also calculated. The values are collected in Table S10 of the ESI.† Fig. 4 illustrates the monomers and dimers, exemplified by H_2O (a) and CH_3COOH (b) with the $\sigma^t(O)$ (in plain) and $\Delta\sigma^t(O)_{dm}$ (in bold) values in ppm, for the better understanding of the discussion. The dimer formation leads to a downfield shift of 7 ppm for H_2O (up to 8 ppm for ROH as shown in Table S10 of the ESI†) and a upfield shift of 49 ppm for C=O* and a downfield shift of 19 ppm for C–O*–H (totally upfield shift by 15 ppm on average) in RCOOH. The analysis for RCOOH would be more complex, since only the averaged data are available due to the interconversion between topological isomers of RCO*OH and RCOO*H. The contribution from HB formation to $\delta(O)$ is well demonstrated, although the direction of the effect may depend on the structures (conformers) of the monomers and dimers.

Fig. 5 shows the plot of $-\Delta\sigma^t(O\text{: S})$ versus $\delta(O\text{: S})$ for the monomers and the dimers of ROH, with and without considering the solvent effect of $CHCl_3$. Table 4 collects the correlations (entries 1N, 2N, 3Y and 4Y). The correlations seem (very) good. They are very similar with each other, especially for the dimers, with and without considering the solvent effect. The apparent solvent effect on $\delta(O\text{: S})$ seems very small, especially for the dimers. The results may show that the monomers and dimers exist (as in equilibrium) in solutions, which controls $\delta(O\text{: S})$ and the solvent effect in ROH. Similarly, $-\Delta\sigma^t(O\text{: S})$ are plotted versus $\delta(O\text{: S})$ for the RCOOH monomers and the dimers, with and without considering the solvent effect, although not shown n a figure. The correlations are shown in Table 4 (entries 5N, 6N, 7Y and 8Y). The correlations become better in the order of (RCOOH monomer: with the solvent effect) $\approx$ (RCOOH monomer: without the solvent effect) $\ll$ (RCOOH dimer: without the solvent effect)
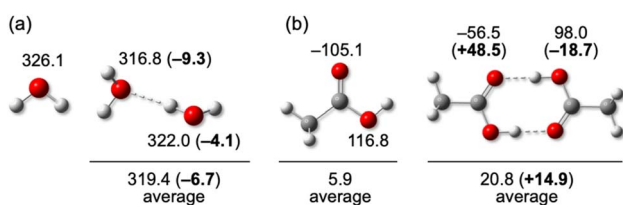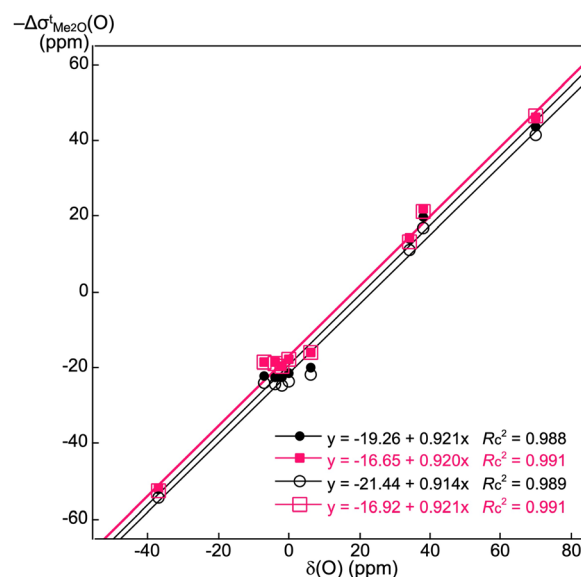

Fig. 5 Plots of calculated $-\Delta\sigma^t(O\text{: S})$ versus observed $\delta(O\text{: S})$ for some monomeric (I) and dimeric (II) alcohols with and without the solvent effect of $CDCl_3$: I with (○) and without (●) the solvent effect and II with (■) and without (□) the solvent effect.

Table 4 Correlations in the plots of calculated $-\Delta\sigma^t(O\text{: S})$ versus observed $\delta(O\text{: S})$ for the monomers and dimers of ROH and ROOH, with and without considering the solvent effect of $CHCl_3$ under B3LYP/BSS-A[a]

Entry[b]	Plot for	a	b	R_c^2	N
1N	ROH monomers	0.921	−19.26	0.988	9
2N	ROH dimers	0.920	−16.65	0.991	9
3Y	ROH monomers	0.914	−21.44	0.989	9
4Y	ROH dimers	0.921	−16.92	0.991	9
5N	RCOOH monomers	0.939	27.29	0.929	5
6N	RCOOH dimers	1.072	−19.76	0.968	5
7Y	RCOOH monomers	0.829	48.25	0.928	5
8Y	RCOOH dimers	0.966	4.03	0.960	5

[a] Observed data are used for the corresponding species in the plot. [b] The solvent effect is specified by N (no solvent effect) or Y (solvent effect) after the entry number.

$\approx$ (RCOOH dimer: with the solvent effect). The dimer formation seems very important in RCOOH, relative to the case of ROH, together with the considering the solvent effect.

After confirming the basic behaviour of $\sigma^t(O)$ for ROR + ROR′, ROH and RCOOH, next extension is to clarify the origin of $\delta(O)$ based on the MO theory. The pre-α, α and β effects, along with the vinyl, carbonyl and carboxyl effects, are analysed using an approximated image, derived from eqn (6).[24]

Origin of the pre-α effect

How are the ^{17}O NMR chemical shifts originated? electrons around a nucleus ^{17}O shield the external magnetic field at the nucleus. The spherical component of the electron distribution arises the diamagnetic terms $\sigma^d(O)$, whereas the paramagnetic terms $\sigma^p(O)$ are originated from the unsymmetrical component

Fig. 4 Illustration of monomers and dimers for H_2O (a) and CH_3COOH (b). The $\sigma^t(O)$ (in plain) and $\Delta\sigma^t(O)_{dm}$ (in bold) values are also shown in ppm.

of the electron distribution. In the case of O^{2-}, only $\sigma^d(O)$ occurs, since the ten electrons in O^{2-} spherically distribute.

The protonation of O^{2-} yields HO^-, which introduces the $\sigma(O–H)$ and $\sigma^*(O–H)$ orbitals, resulting in the unsymmetrical distribution of electrons in HO^-. The spherical electron distribution of O^{2-} changes to an unsymmetrical distribution in HO^-, in this process. As a result, the unsymmetrical component produces $\sigma^p(O)$, although the spherical component arises $\sigma^d(O)$ in HO^-. The $\sigma^p(O)$ terms are caused through the orbital-to-orbital transitions, such as the $\psi_i \rightarrow \psi_a$ transition, where $\sigma(O–H)$ and $\sigma^*(O–H)$ operate as the typical ψ_i and ψ_a, respectively, in the $\psi_i \rightarrow \psi_a$ transition.

We focused our attention to the protonation process on O^{2-} in the NMR analysis as the factor to originate $\sigma^p(O)$. We proposed to call this process the pre-α effect, when the origin of the ^{77}Se NMR chemical shifts were discussed based on $\sigma^p(Se)$.[19] The pre-α effect is very important, since it is the starting point to image the origin of all NMR chemical shifts.

As shown in Scheme 3, the pre-α effect is evaluated by the $(\Delta\sigma^d(O)_e, \Delta\sigma^p(O)_e, \Delta\sigma^t(O)_e)$ values, which are $(-11.7, -19.6, -31.3$ ppm$)$, $(-7.7, -33.4, -41.1$ ppm$)$ and $(-3.7, -31.1, -34.8$ ppm$)$ for the processes from O^{2-} to HO^-, H_2O and H_3O^+, respectively. The values are calculated per unit group (per H in this case). The $\Delta\sigma^t(O)_e$ values are all negative, along with $\Delta\sigma^d(O)_e$ and $\Delta\sigma^p(O)_e$; therefore, the pre-α effect is theoretically predicted to be the downfield shifts of 31–41 ppm ($\Delta\sigma^t(O)_e$) (see also Table 3). The saturation effect in the pre-α effect on $\sigma^d(O)$, $\sigma^p(O)$ and $\sigma^t(O)$ by the increase of the H atoms seems not so severe in this case. Table 5 lists the $\sigma_i^d(O)$, $\sigma_i^p(O)$ and $\sigma_i^t(O)$ $(=\sigma_i^d(O) + \sigma_i^p(O))$ values for O^{2-}, HO^-, H_2O and H_3O^+, which are separately by ψ_i. The 1s (O) AO, in the MOs, predominantly contribute to $\sigma^d(O)$ for each species, whereas the 2s (O), $2p_x$ (O), $2p_y$(O) and $2p_z$(O) AOs do much smaller to $\sigma^d(O)$, as expected. As shown in Table 5, ψ_3 greatly contributes to $\sigma^p(O)$ $(\sigma_3^p(O) = -85.2$ ppm$)$ for HO^-, along with ψ_4 $(-21.9$ ppm$)$ and ψ_5 $(-21.9$ ppm$)$. For H_2O, ψ_3 $(\sigma_3^p(O) = -50.2$ ppm$)$, ψ_4 $(-57.2$ ppm$)$ and ψ_5 $(-63.6$ ppm$)$ greatly contribute to $\sigma^p(O)$. In the case of H_3O^+, ψ_3 $(\sigma_3^p(O) = -43.3$ ppm$)$, ψ_4 $(-43.3$ ppm$)$ and ψ_5 $(-61.9$ ppm$)$ greatly contribute to $\sigma^p(O)$. The three orbitals must mainly be constructed by the $2p_x(O)$, $2p_y(O)$ and $2p_z(O)$ AOs.

Table 6 shows the $\psi_i \rightarrow \psi_a$ transitions predominantly contributing to $\sigma_{i \rightarrow a:xx}^p(O)$, $\sigma_{i \rightarrow a:yy}^p(O)$ and/or $\sigma_{i \rightarrow a:zz}^p(O)$ for HO^- and H_2O, where the three components yield $\sigma_{i \rightarrow a}^p(O)$, according to eqn (2). The magnitudes larger than 6 ppm for $\sigma_{i \rightarrow a}^p(O)$ are provided in Table 6. (The border value for the positive $\sigma_{i \rightarrow a}^p(O)$ values to list the table is usually not specified, since the positive values contribute to the diamagnetic direction.) The $\psi_3 \rightarrow \psi_9$ $(\sigma_{39:xx}^p(O) = -83.9$ ppm$)$, $\psi_3 \rightarrow \psi_{10}$ $(\sigma_{310:zz}^p(O) = -83.9$ ppm$)$, $\psi_4 \rightarrow \psi_8$ $(\sigma_{48:xx}^p(O) = -61.1$ ppm$)$ and $\psi_5 \rightarrow \psi_8$ $(\sigma_{58:zz}^p(O) = -61.1$ ppm$)$ transitions greatly contribute to $\sigma_{i \rightarrow a}^p(O)$ in HO^-. In the case of H_2O, the $\psi_3 \rightarrow \psi_8$ $(\sigma_{38:zz}^p(O) = -28.1$ ppm$)$, $\psi_3 \rightarrow \psi_{11}$ $(\sigma_{311:xx}^p(O) = -32.2$ ppm$)$, $\psi_4 \rightarrow \psi_9$ $(\sigma_{49:zz}^p(O) = -40.9$ ppm$)$, $\psi_5 \rightarrow \psi_8$ $(\sigma_{58:yy}^p(O) = -33.4$ ppm$)$ and $\psi_5 \rightarrow \psi_9$ $(\sigma_{59:xx}^p(O) = -58.8$ ppm$)$ transitions greatly contribute to $\sigma^p(O)$ (see Table 6).

Fig. 5 and 6 illustrate the selected $\psi_i \rightarrow \psi_a$ transitions for HO^- and H_2O, respectively, along with the characteristics of ψ_i and ψ_a and the orbital energies. Fig. 5 shows the $\psi_3 \rightarrow \psi_9$ and $\psi_3 \rightarrow \psi_{10}$

Table 5 The $\sigma^d(O)$, $\sigma^p(O)$ and $\sigma^t(O)$ values contributed from each MO of O^{2-} (**1**), HO^- (**2**), H_2O (**7**) and H_3O^+ (**25**)[a]

MO (i in ψ_i)	$\sigma_i^d(O)$	$\sigma_i^p(O)$	$\sigma_i^t(O)$
O^{2-} (1: O_h)[b,c]			
1	270.67	0.00	270.67
2	43.73	0.00	43.73
3	31.31	0.00	31.31
4	31.31	0.00	31.31
5	31.31	0.00	31.31
Total	408.33	0.00	408.33
HO^- (2: $C_{\infty v}$)			
1	270.64	0.00	270.64
2	39.36	−4.99	34.37
3	17.78	−85.15	−67.36
4	34.41	−21.92	12.49
5	34.41	−21.92	12.49
ψ_{occ} to ψ_{occ}		114.41	
Total	392.85	−19.56	377.03
H_2O (7: C_{2v})			
1	270.61	0.00	270.61
2	38.82	−5.24	33.58
3	18.85	−50.23	−31.38
4	27.35	−57.23	−29.65
5	37.22	−63.55	−26.33
ψ_{occ} to ψ_{occ}		109.30	
Total	392.85	−66.72	326.13
H_3O^+ (25: C_{3v})			
1	270.60	0.00	270.60
2	40.44	−1.93	38.50
3	23.69	−43.31	−19.62
4	23.69	−43.30	−19.61
5	38.77	−61.90	−23.13
ψ_{occ} to ψ_{occ}		57.17	
Total	397.19	−93.28	303.91

[a] Calculated with the GIAO method under B3LYP/BSS-A. [b] The ψ_1, ψ_2, ψ_3, ψ_4 and ψ_5 MOs of O^{2-} correspond to 1s (O), 2s (O), $2p_x$ (O), $2p_y$ (O) and $2p_z$ (O) AOs, respectively. [c] The $\sigma_1^d(O)$, $\sigma_2^d(O)$, $\sigma_3^d(O)$ and $\sigma_4^d(O)$ values of O^0 are evaluated to be 270.67, 45.42, 39.18 and 39.18 ppm, respectively.

transitions in HO^-, which correspond to the transitions from the occupied $\sigma(O–H)$ orbital to the vacant $3p_z$ and $3p_x$ orbitals, respectively, where $3p_z$ and $3p_x$ are equivalent in HO^-. The $\psi_4 \rightarrow \psi_8$ and $\psi_5 \rightarrow \psi_8$ transitions correspond to the transitions from the occupied $2p_z$ and $2p_x$ orbitals to the vacant orbitals containing the $\sigma^*(O–H)$ character, respectively. The occupied $\sigma(O–H)$ and vacant $\sigma^*(O–H)$ orbitals operate as the typical donor and acceptor orbitals, respectively, in the transitions to produce the $\sigma_{i \rightarrow a}^p(O)$ terms.

The $\sigma(O–H)$ and $\sigma^*(O–H)$ orbitals in H_2O similarly act as the typical donor and acceptor orbitals, respectively, according to the C_{2v} symmetry of H_2O, as shown in Fig. 6. The ψ_3 (B2)$\rightarrow \psi_8$ (A1) and ψ_3 (B2)$\rightarrow \psi_{11}$ (B1) transitions correspond to the occupied $\sigma(H–O–H)$ orbital to the vacant orbitals containing the $\sigma^*(H–O–H)$ and $3p_z(O)$ characters, respectively. While the ψ_4 (A1)$\rightarrow \psi_9$ (B2) transition corresponds to the occupied $n_s(O)$ orbital to the vacant orbital containing the $\sigma^*(H–O–H)$ character, ψ_5 (B1) in the ψ_5 (B1)$\rightarrow \psi_8$ (A1) and ψ_5 (B1)$\rightarrow \psi_9$ (B2)

Table 6 Main contributions from the occupied-to-unoccupied orbital transitions on $\sigma^{\mathrm{P}}(O)$ for HO^- (**2**) and H_2O (**7**)[a]

$i \rightarrow a$[b]	$\sigma^{\mathrm{P}}_{i \rightarrow a:xx}(O)$	$\sigma^{\mathrm{P}}_{i \rightarrow a:yy}(O)$	$\sigma^{\mathrm{P}}_{i \rightarrow a:zz}(O)$	$\sigma^{\mathrm{P}}_{i \rightarrow a}(O)$
HO$^-$ (2: $C_{\infty v}$)				
$3 \rightarrow 9$	−83.87	0.00	0.00	−27.96
$3 \rightarrow 10$	0.00	0.00	−83.87	−27.96
$3 \rightarrow 22$	0.00	0.00	−18.14	−6.05
$3 \rightarrow 23$	−18.14	0.00	0.00	−6.05
$4 \rightarrow 6$	21.65	0.00	0.00	7.22
$4 \rightarrow 7$	40.70	0.00	0.00	13.57
$4 \rightarrow 8$	−61.09	0.00	0.00	−20.36
$4 \rightarrow 14$	−35.47	0.00	0.00	−11.82
$5 \rightarrow 6$	0.00	0.00	21.65	7.22
$5 \rightarrow 7$	0.00	0.00	40.70	13.57
$5 \rightarrow 8$	0.00	0.00	−61.09	−20.36
$5 \rightarrow 14$	0.00	0.00	−35.47	−11.82
H$_2$O (7: C_{2v})				
$3 \rightarrow 8$	0.00	0.00	−28.12	−9.37
$3 \rightarrow 11$	−32.22	0.00	0.00	−10.74
$4 \rightarrow 9$	0.00	0.00	−40.87	−13.62
$4 \rightarrow 11$	0.00	−21.09	0.00	−7.03
$4 \rightarrow 13$	0.00	0.00	−18.69	−6.23
$4 \rightarrow 17$	0.00	0.00	−25.65	−8.55
$5 \rightarrow 6$	0.00	−23.27	0.00	−7.76
$5 \rightarrow 8$	0.00	−33.37	0.00	−11.12
$5 \rightarrow 9$	−58.81	0.00	0.00	−19.60
$5 \rightarrow 17$	−32.49	0.00	0.00	−10.83
$5 \rightarrow 18$	0.00	−18.91	0.00	−6.30
$5 \rightarrow 21$	−18.69	0.00	0.00	−6.23

[a] Calculated with the GIAO method under B3LYP/BSS-A. The magnitudes of $\sigma^{\mathrm{P}}_{i \rightarrow a}(O)$ larger than 6 ppm are shown. [b] In $\psi_i \rightarrow \psi_a$.
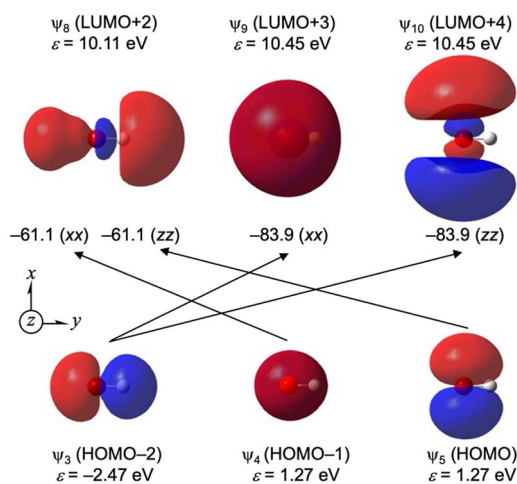

Fig. 6 Main contributions from each $\psi_i \rightarrow \psi_a$ transition to the components of $\sigma^{\mathrm{P}}(O)$ in HO^- (**2**).

transitions has the characters of the occupied $n_p(O)$ ($2p_z(O)$) orbital. As observed, the $\sigma(O-H)$ orbitals in H_2O act as the typical donors in the combined form of C_{2v}, together with $2p_z(O)$, while the $\sigma^*(O-H)$ orbitals operate as the typical acceptors in the transition, although the character seems to fractionalize to some vacant orbitals, containing the higher $3p_z(O)$ orbital (Fig. 7).
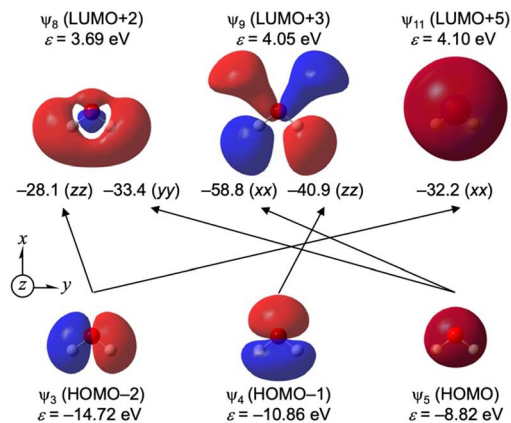

Fig. 7 Main contributions from each $\psi_i \rightarrow \psi_a$ transition to the components of $\sigma^{\mathrm{P}}(O)$ in H_2O (**7**).

Origin of the α effect

The α effect is evaluated for MeOH, Me$_2$O and MeO$^+$H$_2$, using $(\Delta\sigma^{\mathrm{d}}(O)_e, \Delta\sigma^{\mathrm{P}}(O)_e, \Delta\sigma^{\mathrm{t}}(O)_e)$, of which values are (2.2, −6.2, −3.9 ppm), (1.6, −3.3, −1.7 ppm) and (3.2, −1.6, −1.6 ppm), respectively. The magnitudes of $\Delta\sigma^{\mathrm{t}}(O)_e$ are small in magnitudes (less than 4 ppm). The signs of $\Delta\sigma^{\mathrm{d}}(O)_e$ and $\Delta\sigma^{\mathrm{P}}(O)_e$ are just inverse, where $\Delta\sigma^{\mathrm{t}}(O)_e = \Delta\sigma^{\mathrm{d}}(O)_e + \Delta\sigma^{\mathrm{P}}(O)_e$; this is likely the reason for the small α effect predicted based on $\Delta\sigma^{\mathrm{t}}(O)_e$. In the case of MeO$^-$ from OH$^-$, the $(\Delta\sigma^{\mathrm{d}}(O)_e, \Delta\sigma^{\mathrm{P}}(O)_e, \Delta\sigma^{\mathrm{t}}(O)_e)$ values are (18.5, −114.3, −95.8 ppm). The large magnitude for $\Delta\sigma^{\mathrm{t}}(O)_e$ comes from the large magnitude of $\Delta\sigma^{\mathrm{P}}(O)_e$, where the negative charge on MeO$^-$ would contribute to the results.

The large upfield shifts observed in ROH as the α effect appear to be difficult to explain based on the calculated $\Delta\sigma^{\mathrm{t}}(O)_e$ values, under the calculation conditions employed in this work. The contribution from HB formation and/or the solvent effect under the observed conditions would be responsible for this.

Table 7 lists the $\sigma^{\mathrm{d}}_i(O)$, $\sigma^{\mathrm{P}}_i(O)$ and $\sigma^{\mathrm{t}}_i(O)$ ($=\sigma^{\mathrm{d}}_i(O) + \sigma^{\mathrm{P}}_i(O)$) values, separately by ψ_i, for Me$_2$O. The inner orbital of ψ_1 is constructed by the 1s (O) AO; therefore, it greatly contributes to $\sigma^{\mathrm{d}}(O)$ but does not contribute to $\sigma^{\mathrm{P}}(O)$. Those of ψ_2 and ψ_3 are constructed by the two 1s (C) AOs; therefore, the contributions to $\sigma^{\mathrm{d}}(O)$ and $\sigma^{\mathrm{P}}(O)$ are very minimal. ψ_5, ψ_6, ψ_{10} and ψ_{11} are mainly constructed by the 2s (C) and 2p (C) AOs; therefore, the contributions to $\sigma^{\mathrm{d}}(O)$ and $\sigma^{\mathrm{P}}(O)$ are also minimal. The contributions from ψ_7–ψ_9 and ψ_{12} to $\sigma^{\mathrm{P}}_i(O)$ are large (−31 to −69 ppm), where ψ_7–ψ_9 and ψ_{12} are mainly formed by the 2p (O) AOs. The contributions from ψ_4 and ψ_{13} to $\sigma^{\mathrm{P}}_i(O)$ are −13.1 and −17.9 ppm, respectively, where ψ_4 and ψ_{13} are mainly constructed by both 2s (O) and 2p (O) AOs. As shown in Table 8, the $\psi_8 \rightarrow \psi_{34}$ ($\sigma^{\mathrm{P}}_{834:zz}(O) = -44.9$ ppm), $\psi_9 \rightarrow \psi_{34}$ ($\sigma^{\mathrm{P}}_{934:xx}(O) = -48.0$ ppm), $\psi_{12} \rightarrow \psi_{37}$ ($\sigma^{\mathrm{P}}_{1237:zz}(O) = -69.4$ ppm) and $\psi_{12} \rightarrow \psi_{51}$ ($\sigma^{\mathrm{P}}_{1251:zz}(O) = -51.6$ ppm) transitions greatly contribute to the components of $\sigma^{\mathrm{P}}(O)$ in Me$_2$O.

Fig. 8 shows the selected $\psi_i \rightarrow \psi_a$ transitions in Me$_2$O; these are considered to be the effective transitions. Both occupied and vacant orbitals extend over the entire molecule. Whereas ψ_{12} (HOMO−1) of the $n_s(O)$ type acts as a good donor in Me$_2$O, the

Table 7 The $\sigma^d(O)$, $\sigma^p(O)$ and $\sigma^t(O)$ values contributed from each MO of Me$_2$O (**14**: C_{2v})^a

MO (i in ψ_i)	$\sigma_i^d(O)$	$\sigma_i^p(O)$	$\sigma_i^t(O)$
1	270.62	0.00	270.62
2,3	0.06	0.12	0.18
4	33.03	−13.07	19.96
5	9.48	4.29	13.77
6	9.14	1.85	10.99
7	11.54	−31.13	−19.59
8	9.46	−40.02	−30.56
9	10.83	−47.49	−36.66
10	−1.00	−2.70	−3.71
11	0.33	7.11	8.11
12	13.25	−68.58	−55.33
13	29.39	−17.93	11.46
ψ_{occ} to ψ_{occ}		133.50	
Total	396.11	−73.37	322.75

^{a} Calculated with the GIAO method under B3LYP/BSS-A.

Table 8 Main contributions from occupied-to-unoccupied orbital transitions on $\sigma^p(O)$ of Me$_2$O (**14**: C_{2v})^{a,b}

$i \to a^b$	$\sigma_{i \to a:xx}^p(O)$	$\sigma_{i \to a:yy}^p(O)$	$\sigma_{i \to a:zz}^p(O)$	$\sigma_{i \to a}^p(O)$
7 → 30	0.00	0.00	−25.63	−8.54
8 → 34	0.00	0.00	−44.88	−14.96
8 → 37	0.00	0.00	−22.04	−7.35
9 → 34	−47.96	0.00	0.00	−15.99
11 → 28	0.00	0.00	18.47	6.16
11 → 30	0.00	0.00	25.08	8.36
12 → 15	0.00	0.00	−22.81	−7.60
12 → 26	0.00	0.00	−37.56	−12.45
12 → 29	0.00	−21.18	0.00	−7.06
12→37	0.00	0.00	−69.38	−23.13
12 → 38	0.00	0.00	−18.72	−6.24
12 → 51	0.00	0.00	−51.56	−17.19
13 → 14	0.00	−29.14	0.00	−9.71
13 → 15	−45.67	0.00	0.00	−15.22
13 → 18	0.00	24.35	0.00	8.12
13 → 23	34.67	0.00	0.00	11.56
13 → 26	−51.91	0.00	0.00	−17.30
13 → 28	0.00	60.24	0.00	20.08
13 → 30	0.00	−51.05	0.00	−17.02
13 → 34	67.28	0.00	0.00	22.43
13 → 39	0.00	−25.91	0.00	−8.64
13 → 51	−39.27	0.00	0.00	−13.09
13 → 55	38.17	0.00	0.00	12.72

^{a} Calculated with the GIAO method under B3LYP/BSS-A. The magnitudes of $\sigma_{i \to a}^p(O)$ larger than 6 ppm are shown. ^{b} In $\psi_i \to \psi_a$.

Fig. 8 Main contributions from each $\psi_i \to \psi_a$ transition to the components of $\sigma^p(O)$ in Me$_2$O (**14**: C_{2v}).

Origin of the β effect

The β effect is discussed first for ROH, ROMe and ROR, where R changes from Me to Et, then i-Pr, and then t-Bu. The calculated ($\Delta\sigma^d(O)_e$, $\Delta\sigma^p(O)_e$, $\Delta\sigma^t(O)_e$) values are (−0.4 ∼ 4.7, −43.4 ∼ −20.6, −38.8 ∼ −19.8 ppm) for the processes (see Table 3 and Scheme 3). The magnitudes of $\Delta\sigma^d(O)_e$ are less than 5 ppm (usually positive), while the $\Delta\sigma^p(O)_e$ and $\Delta\sigma^t(O)_e$ values are approximately −40 ∼ −20 ppm. Specifically, the β effect is recognized as the downfield shift of 40∼20 ppm, based on the calculations; this effectively explains the observed effect. Similar results are predicted for the processes from MeOH$_2^+$ to EtOH$_2^+$ ($\Delta\sigma^t(O)_e = -29.7$ ppm) and from Me$_3$OH$^+$ to Et$_3$OH$^+$

Table 9 The $\sigma^d(O)$, $\sigma^p(O)$ and $\sigma^t(O)$ values contributed from each MO of Et$_2$O (**20**: C_{2v})^a

MO (i in ψ_i)	$\sigma_i^d(O)$	$\sigma_i^p(O)$	$\sigma_i^t(O)$
1	270.61	0.00	270.61
2–5	0.11	0.25	0.35
6	33.53	−8.62	24.91
7	8.26	3.14	11.39
8	5.77	−0.96	4.81
9	3.90	−6.62	−2.71
10	8.46	−0.72	7.74
11	6.58	−59.26	−52.68
12	8.50	−34.89	−26.40
13	0.79	−2.06	−1.28
14	4.31	−36.72	−32.41
15	0.08	−12.83	−12.74
16	2.96	−20.13	−17.17
17	4.94	−13.49	−8.56
18	−0.22	−0.06	−0.28
19	−2.57	−4.12	−6.69
20	12.47	−52.83	−40.36
21	28.38	−29.12	−0.74
ψ_{occ} to ψ_{occ}		142.90	
Total	396.85	−136.13	260.72

^{a} Using the GIAO method under B3LYP/BSS-A.

vacant orbitals around ψ_{14} (LUMO) do not operate as the effective acceptors in the transitions. The high electronegativity of O, relative to C, potentially prevents the contribution of 2p (O) in the vacant orbitals around the LUMO. AOs on the higher electronegative atoms are tend to contribute in the occupied MOs but not in the vacant MOs. The large contributions from the vacant orbitals around LUMO to $\Delta\sigma^p(O)_e$ are predicted for the formation of MeO$^-$ from HO$^-$, where the high electronegativity of O would be relaxed by the negative charge.
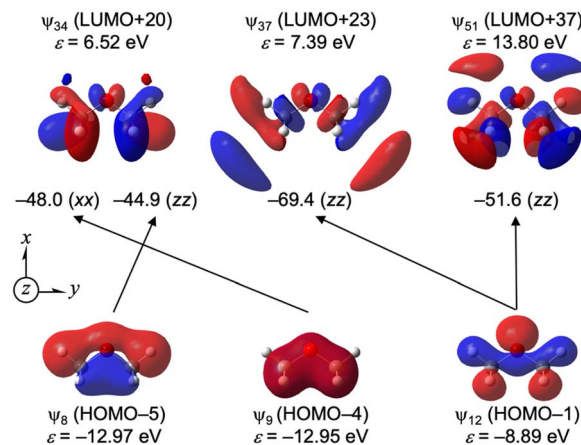
$(\Delta\sigma^{\mathrm{t}}(\mathrm{O}))_{\mathrm{e}} = -19.6$ ppm). In the case of the processes from MeO$^-$ to EtO$^-$, then i-PrO$^-$ and then t-BuO$^-$, the $(\Delta\sigma^{\mathrm{d}}(\mathrm{O})_{\mathrm{e}}, \Delta\sigma^{\mathrm{p}}(\mathrm{O})_{\mathrm{e}}, \Delta\sigma^{\mathrm{t}}(\mathrm{O})_{\mathrm{e}})$ values are $(4.4, -156.7, -152.3$ ppm$)$, $(4.2, -81.8, -77.6$ ppm$)$ and $(4.2, -31.2, -27.0$ ppm$)$, respectively. The magnitudes of $\Delta\sigma^{\mathrm{p}}(\mathrm{O})_{\mathrm{e}}$ and $\Delta\sigma^{\mathrm{t}}(\mathrm{O})_{\mathrm{e}}$ decrease in the order of $CH_3 > CH_2 > CH$, of which H is substituted by Me. The large negative values of $\Delta\sigma^{\mathrm{p}}(\mathrm{O})_{\mathrm{e}}$ (and $\Delta\sigma^{\mathrm{t}}(\mathrm{O})_{\mathrm{e}}$) lead to the large β effect in EtO$^-$ and i-PrO$^-$, while the effect for t-BuO$^-$ appears normal.

Table 9 lists the $\sigma^{\mathrm{d}}(\mathrm{O})$, $\sigma^{\mathrm{p}}(\mathrm{O})$ and $\sigma^{\mathrm{t}}(\mathrm{O})$ values, separately by ψ_i, exemplified by Et_2O (C_{2v}). The contributions from ψ_{11}, ψ_{12}, ψ_{14}, ψ_{20} and ψ_{21} to $\sigma_i^{\mathrm{p}}(\mathrm{O})$ are large ($-29.1 \sim -59.3$ ppm). Table 10 shows the main $\psi_i \rightarrow \psi_a$ transitions, contributing to $\sigma_{i\rightarrow a:xx}^{\mathrm{p}}(\mathrm{O})$, $\sigma_{i\rightarrow a:yy}^{\mathrm{p}}(\mathrm{O})$, or $\sigma_{i\rightarrow a:zz}^{\mathrm{p}}(\mathrm{O})$. The main transitions are $\psi_{14} \rightarrow \psi_{57}$ $(\sigma_{14\bar{5}7:zz}^{\mathrm{p}}(\mathrm{O}) = -31.2$ ppm), $\psi_{14} \rightarrow \psi_{88}$

$(\sigma_{14\bar{8}8:zz}^{\mathrm{p}}(\mathrm{O}) = -43.8$ ppm$)$, $\psi_{20} \rightarrow \psi_{83}$ $(\sigma_{20\bar{8}3:zz}^{\mathrm{p}}(\mathrm{O}) = -37.8$ ppm$)$, $\psi_{20} \rightarrow \psi_{85}$ $(\sigma_{20\bar{8}5:zz}^{\mathrm{p}}(\mathrm{O}) = -37.5$ ppm$)$, $\psi_{21} \rightarrow \psi_{22}$ $(\sigma_{21\bar{2}2:yy}^{\mathrm{p}}(\mathrm{O}) = -53.9$ ppm$)$, $\psi_{21} \rightarrow \psi_{37}$ $(\sigma_{21\bar{3}7:yy}^{\mathrm{p}}(\mathrm{O}) = -36.6$ ppm$)$, $\psi_{21} \rightarrow \psi_{44}$ $(\sigma_{21\bar{4}4:yy}^{\mathrm{p}}(\mathrm{O}) = -30.1$ ppm$)$ and $\psi_{21} \rightarrow \psi_{57}$ $(\sigma_{21\bar{5}7:xx}^{\mathrm{p}}(\mathrm{O}) = -35.0$ ppm$)$, together with $\psi_{21} \rightarrow \psi_{54}$ $(\sigma_{21\bar{5}4:yy}^{\mathrm{p}}(\mathrm{O}) = 52.0$ ppm$)$ and $\psi_{21} \rightarrow \psi_{58}$ $(\sigma_{21\bar{5}8:xx}^{\mathrm{p}}(\mathrm{O}) = 49.1$ ppm$)$, which contribute to the diamagnetic direction.

Fig. 9 draws the selected $\psi_i \rightarrow \psi_a$ transitions in Et_2O, together with the characters of ψ_i and ψ_a and the orbital energies. It is expected to clarify the mechanisms for the β effect. Similar to the case of Me_2O, the occupied and vacant orbitals in Et_2O extend over the whole molecule. It is also curious that the vacant orbitals around ψ_{22} (LUMO) do not operate effectively as acceptors in the transitions. However, the ethyl groups in Et_2O

Table 10 Main contributions from the $\psi_{\mathrm{occ}} \rightarrow \psi_{\mathrm{unocc}}$ transitions on $\sigma^{\mathrm{p}}(\mathrm{O})$ in Et_2O (20: C_{2v})[a]

$i \rightarrow a$[b]	$\sigma_{i\rightarrow a:xx}^{\mathrm{p}}(\mathrm{O})$	$\sigma_{i\rightarrow a:yy}^{\mathrm{p}}(\mathrm{O})$	$\sigma_{i\rightarrow a:zz}^{\mathrm{p}}(\mathrm{O})$	$\sigma_{i\rightarrow a}^{\mathrm{p}}(\mathrm{O})$	$i \rightarrow a$[b]	$\sigma_{i\rightarrow a:xx}^{\mathrm{p}}(\mathrm{O})$	$\sigma_{i\rightarrow a:yy}^{\mathrm{p}}(\mathrm{O})$	$\sigma_{i\rightarrow a:zz}^{\mathrm{p}}(\mathrm{O})$	$\sigma_{i\rightarrow a}^{\mathrm{p}}(\mathrm{O})$
11 → 34	0.00	0.00	−19.97	−6.66	20 → 65	0.00	0.00	−19.34	−6.45
11 → 64	0.00	0.00	−18.68	−6.23	20 → 83	0.00	0.00	−37.75	−12.58
12 → 57	−24.38	0.00	0.00	−8.13	20 → 85	0.00	0.00	−37.45	−12.48
12 → 58	−21.43	0.00	0.00	−7.14	21 → 22	0.00	−53.89	0.00	−17.96
14 → 57	0.00	0.00	−31.15	−10.38	21 → 37	0.00	−36.58	0.00	−12.19
14 → 58	0.00	0.00	−29.21	−9.74	21 → 44	0.00	−30.09	0.00	−10.03
14 → 88	0.00	0.00	−43.76	−14.59	21→54	0.00	52.02	0.00	17.34
15 → 58	0.00	0.00	−23.00	−7.67	21 → 55	0.00	−19.12	0.00	−6.37
16 → 58	−30.60	0.00	0.00	−10.20	21 → 57	−34.98	0.00	0.00	−11.66
17 → 51	−17.84	0.00	0.00	−5.95	21 → 58	49.06	0.00	0.00	16.35
17→ 54	0.00	0.00	−24.15	−8.05	21 → 64	0.00	−28.92	0.00	−9.64
20 → 51	0.00	−29.16	0.00	−9.72	21 → 83	−29.31	0.00	0.00	−9.77

[a] Calculated with the GIAO method under B3LYP/BSS-A. The magnitudes of $\sigma_{i\rightarrow a}^{\mathrm{p}}(\mathrm{O})$ larger than 6 ppm are shown. [b] In $\psi_i \rightarrow \psi_a$.
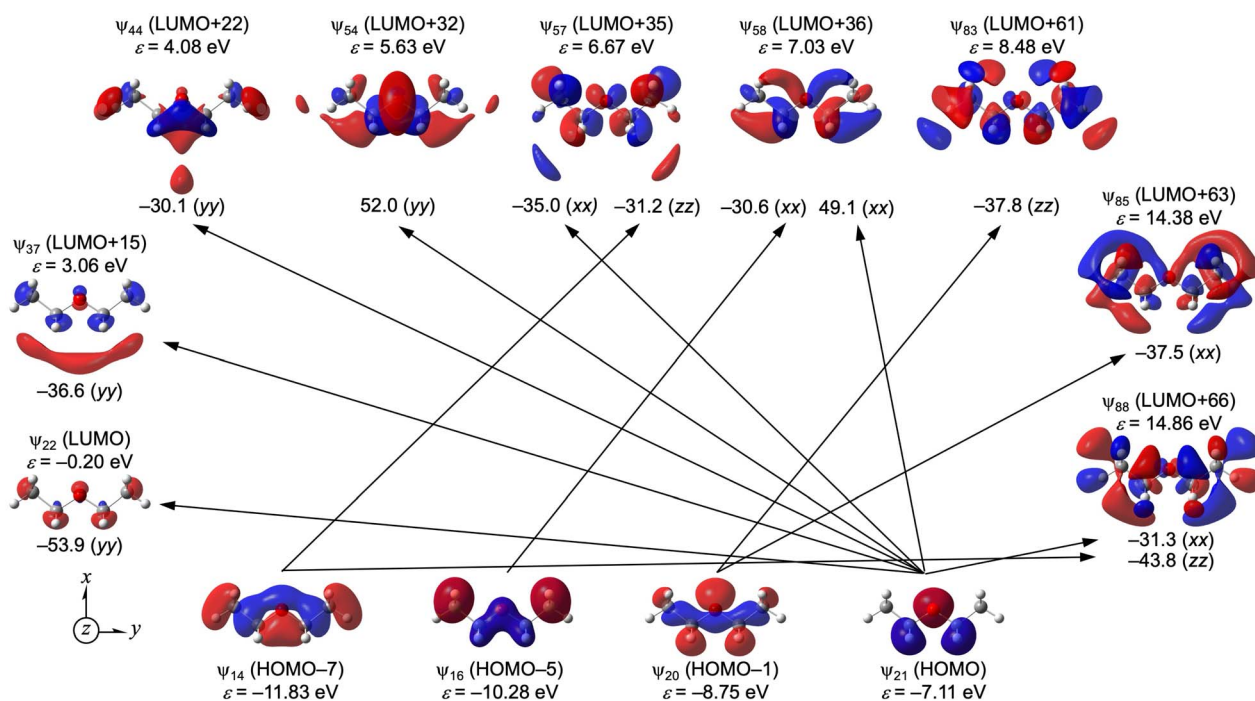

Fig. 9 Main contributions from each $\psi_i \rightarrow \psi_a$ transition to the components of $\sigma^{\mathrm{p}}(\mathrm{O})$ in Et_2O (20).

seem to play an important role in the (large) β effect, contrary to the case of the Me groups in Me$_2$O, which seem not to play an important role in the α effect, for example.

In the case of Et$_2$O, ψ_{11}, ψ_{12}, ψ_{14}, ψ_{20} and ψ_{21} contribute to $\sigma^P(O)$, over ∼30 ppm in magnitude and the $\sigma^P(O)$ value is −136.1 ppm, as the total contribution. The contributions in Et$_2$O are compared with those in Me$_2$O and H$_2$O. The ψ_7, ψ_8, ψ_9 and ψ_{12} orbitals in Me$_2$O contribute to $\sigma^P(O)$, over 30 ppm in magnitude and the $\sigma^P(O)$ values −73.4 ppm, as the total contribution. In the case of H$_2$O, ψ_3, ψ_4 and ψ_5 contribute to $\sigma^P(O)$, over 50 ppm in magnitude, which leads to the total contribution of $\sigma^P(O)$ of −66.7 ppm. The $\sigma^P(O)$ values of (Me$_2$O from H$_2$O) and (Et$_2$O from Me$_2$O) are calculated to be −3.3 and −31.4 ppm (per Me), respectively. The values correspond to the minimal α effect in Me$_2$O and the large β effect in Et$_2$O, in magnitudes, based on the calculations. The minimal α effect potentially originates from the cancelling of many (complex) transitions to produce $\sigma^P(O)$, while this cancelling would be avoided in the β effect.

Origin of the γ and δ effects

The upfield shifts of 1.7, 2.8 and 2.4 ppm by $\Delta\sigma^t(O)_e$ were predicted for the γ effect in the formation of n-PrOH from EtOH, n-PrOMe from EtOMe and n-Pr$_2$O from Et$_2$O, respectively. Similarly, the upfield shifts of 0.8, 0.3 and 0.8 ppm by $\Delta\sigma^t(O)_e$ are for the δ effect in n-BuOH formed from n-PrOH, n-BuOMe from n-PrOMe and n-Bu$_2$O from n-Pr$_2$O, respectively. The predicted magnitudes of $\Delta\sigma^t(O)_e$ are very small. The magnitudes of $\Delta\sigma^d(O)_e$ and $\Delta\sigma^P(O)_e$ are also very small, and the signs are the inverse to each other. The mechanisms for the γ and δ effects are not analysed further, due to the negligibly small magnitudes.

Effect from the vinyl group

Large downfield shifts in $\delta(^{17}O)$ (∼80 ppm) are reported for vinyl ethers.[49] The effect from the vinyl group is calculated, exemplified by the process from EtOH to H$_2$C=CHOH (C_s), although the process can be diversely described. The ($\Delta\sigma^d(O)_e$, $\Delta\sigma^P(O)_e$, $\Delta\sigma^t(O)_e$) values for the process are calculated to be (4.4, −85.5, −81.1 ppm), which effectively reproduced the observed results.

Table 11 lists the $\sigma^d(O)$, $\sigma^P(O)$ and $\sigma^t(O)$ values of H$_2$C=CHOH (C_s), separately by ψ_i. The contributions from ψ_7, ψ_{10} and ψ_{11} to $\sigma_i^P(O)$ are (very) large, of which values are −48.0, −67.3 and −56.9 ppm, respectively. As shown in Table 12, the $\psi_{10} \to \psi_{30}$ ($\sigma^P_{10\bar{3}0:xx}(O) = -21.3$ ppm and $\sigma^P_{10\bar{3}0:yy}(O) = -28.7$ ppm) and $\psi_{11} \to \psi_{14}$ ($\sigma^P_{1\bar{1}14:xx}(O) = -175.5$ ppm) transitions provide great contributions.

Fig. 10 illustrates the $\psi_i \to \psi_a$ transitions in H$_2$C=CHOH (C_s) with the axes. The main characters of ψ_{10}, ψ_{11}, ψ_{14} and ψ_{30} are the occupied π(C=C–O), occupied n_s(O), vacant π*(C=C–O) and vacant σ*(C=C–O) orbitals, respectively, and they extend over the entire molecule. For the large $\sigma^P(O)$ values in H$_2$C = CHOH (C_s), ψ_{10} (π(C=C–O)) and ψ_{11}(n_s(O)) act as excellent donors, while ψ_{14} (π*(C=C–O)) and ψ_{30} (σ*(C=C–O)) operate as good acceptors. In particular, the ψ_{11} (HOMO−1) → ψ_{14} (LUMO+1) transition greatly contributes to $\sigma^P_{1\bar{1}14}(O)$ of −58.0 ppm.

Table 11 The $\sigma^d(O)$, $\sigma^P(O)$ and $\sigma^t(O)$ values of H$_2$Ce001CHOH (**31**: C_s), given separately by each ψ_i[a]

MO (i in ψ_i)	$\sigma_i^d(O)$	$\sigma_i^P(O)$	$\sigma_i^t(O)$
1	270.61	0.00	270.61
2	0.02	0.05	0.08
3	0.01	0.01	0.02
4	36.10	−6.49	29.61
5	5.35	4.45	9.80
6	10.22	−14.77	−4.55
7	9.55	−48.00	−38.45
8	9.56	−23.28	−13.71
9	6.00	−18.04	−12.04
10	28.45	−67.27	−38.82
11	17.59	−56.91	−39.32
12	9.29	4.93	14.22
ψ_{occ} to ψ_{occ}		31.50	
Total	402.75	−193.80	208.95

[a] Using the GIAO method under B3LYP/BSS-A.

Table 12 Main contributions from occupied-to-unoccupied orbital transitions on $\sigma^P(O)$ of H$_2$C=CHOH (**31**: C_s)[a]

$i \to a$[b]	$\sigma^P_{i \to a:xx}(O)$	$\sigma^P_{i \to a:yy}(O)$	$\sigma^P_{i \to a:zz}(O)$	$\sigma^P_{i \to a}(O)$
6 → 14	−0.15	−34.97	0.00	−11.70
7 → 29	−0.29	−21.78	0.00	−7.36
7 → 30	0.00	0.00	−18.56	−6.19
8 → 14	19.02	−54.77	0.00	−11.92
10 → 30	−21.27	−28.67	0.00	−16.65
10 → 31	0.25	−23.28	0.00	−7.68
11 → 13	0.00	0.00	−23.14	−7.71
11 → 14	−175.47	1.34	0.00	−58.04
11 → 30	0.00	0.00	44.83	14.94
11 → 46	0.00	0.00	−27.56	−9.19
12 → 13	5.81	−23.50	0.00	−5.90
12 → 30	15.83	32.73	0.00	16.18

[a] Calculated with the GIAO method under B3LYP/BSS-A. The magnitudes of $\sigma^P_{i \to a}(O)$ larger than 6 ppm are shown. [b] In $\psi_i \to \psi_a$.

Effect from the carbonyl group

Very large downfield shifts in $\delta(^{17}O)$ (200–400 ppm) are reported for the species containing the carbonyl group.[50] The mechanisms are discussed, exemplified by the formation of H$_2$C=O from MeOH, first.

Table 13 lists the $\sigma^d(O)$, $\sigma^P(O)$ and $\sigma^t(O)$ values of H$_2$C=O, separately by ψ_i. The contributions from ψ_6 and ψ_8 on $\sigma_i^P(O)$ are very large, which amount to −264.8 and −480.4 ppm, respectively. The ($\Delta\sigma^d(O)_e$, $\Delta\sigma^P(O)_e$, $\Delta\sigma^t(O)_e$) values are (9.4, −760.9, −751.5 ppm) for H$_2$C=O from MeOH. As shown in Table 14, the $\psi_6 \to \psi_9$ ($\sigma^P_{69:yy}(O) = -647.6$ ppm) and $\psi_8 \to \psi_9$ ($\sigma^P_{89:xx}(O) = -1385.1$ ppm) transitions are the predominant contributors.

Fig. 11 illustrates the selected $\psi_i \to \psi_a$ transitions of $\psi_6 \to \psi_9$ and $\psi_8 \to \psi_9$ in H$_2$C=O, along with the molecular axes. The ψ_6, ψ_8 and ψ_9 orbitals mainly have the occupied σ(C=O), occupied n_{py}(O) and vacant π*(C=O) characters, respectively. The ψ_6 (σ(C=O)) and ψ_8 (n_{py}(O)) orbitals act as excellent donors, while
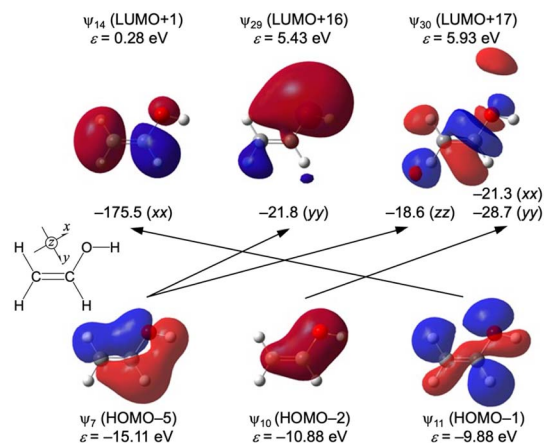
Fig. 10 Main contributions from each $\psi_i \rightarrow \psi_a$ transition to the components of $\sigma^P(O)$ in $H_2C=CHOH$ (**31**), with the axes.

Table 13 The $\sigma^d(O)$, $\sigma^P(O)$ and $\sigma^t(O)$ values of $H_2C=O$ (**34**: C_{2v}), given separately by each $\psi_i{}^a$

MO (i in ψ_i)	$\sigma_i^d(O)$	$\sigma_i^P(O)$	$\sigma_i^t(O)$
1	270.61	0.00	270.61
2	0.03	0.05	0.08
3	32.51	−25.86	6.65
4	8.91	8.95	17.87
5	10.38	9.93	20.31
6	25.20	−264.75	−239.55
7	28.07	−41.88	−13.81
8	28.79	−480.42	−451.63
ψ_{occ} to ψ_{occ}		−39.79	
Total	404.50	−833.77	−429.27

^{a} Using the GIAO method under B3LYP/BSS-A.

Table 14 Main contributions from occupied-to-unoccupied orbital transitions on $\sigma^P(O)$ of $H_2C=O$ (**34**: C_{2v})^a

$i \rightarrow a^b$	$\sigma_{i \rightarrow a:xx}^P(O)$	$\sigma_{i \rightarrow a:yy}^P(O)$	$\sigma_{i \rightarrow a:zz}^P(O)$	$\sigma_{i \rightarrow a}^P(O)$
$3 \rightarrow 9$	0.00	−37.45	0.00	−12.48
$5 \rightarrow 9$	93.99	0.00	0.00	31.33
$6 \rightarrow 9$	0.00	−647.61	0.00	−215.87
$6 \rightarrow 18$	0.00	0.00	−38.06	−12.69
$7 \rightarrow 33$	0.00	−31.32	0.00	−10.44
$8 \rightarrow 9$	−1385.05	0.00	0.00	−461.68
$8 \rightarrow 10$	0.00	0.00	−40.47	−13.49
$8 \rightarrow 13$	−43.55	0.00	0.00	−14.52
$8 \rightarrow 19$	−31.54	0.00	0.00	−10.51
$8 \rightarrow 33$	0.00	0.00	38.09	12.70

^{a} Calculated with the GIAO method under B3LYP/BSS-A. The magnitudes of $\sigma_{i \rightarrow a}^P(O)$ larger than 10 ppm are shown. ^{b} In $\psi_i \rightarrow \psi_a$.

ψ_9 ($\pi^*(C=O)$) does as an excellent acceptor to produce the very large $\sigma^P(O)$ in $H_2C=O$. However, ψ_7 ($\pi(C=O)$) seems not a good donor in the transitions, relative to the case of ψ_6 and ψ_8.

The origin for the very large downfield shift for $\sigma^P(O: H_2C=O)$ is effectively analysed, along with the mechanism.

Effect from the carboxyl group

The carboxyl effect is closely related to the carbonyl effect, which is discussed for the formation of $H(HO^*)C=O^*$ from MeOH.

Table 15 lists the $\sigma^d(O)$, $\sigma^P(O)$ and $\sigma^t(O)$ values of $H(HO)C=O^*$ and $H(HO^*)C=O$, separately by ψ_i. The contributions from ψ_{10} and ψ_{12} to $\sigma_i^P(O)$ are very large for $H(HO)C=O^*$, which amounts to −130.4 and −234.1 ppm, respectively, while that from ψ_{10} to $\sigma_i^P(O)$ is also very large for $H(HO^*)C=O$, which amounts to −120.2 ppm. Table 16 shows the $\psi_i \rightarrow \psi_a$ transitions, mainly contributing to $\sigma_{i \rightarrow a:xx}^P(O)$, $\sigma_{i \rightarrow a:yy}^P(O)$ and/or $\sigma_{i \rightarrow a:zz}^P(O)$, in $H(HO)C=O^*$ and $H(HO^*)C=O$. In the case of $H(HO)C=O^*$, the $\psi_{10} \rightarrow \psi_{13}$ ($\sigma_{10\bar{1}3:yy}^P(O) = -279.3$ ppm; $\sigma_{10\bar{1}3:xx}^P(O) = -45.9$ ppm) and $\psi_{12} \rightarrow \psi_{13}$ ($\sigma_{12\bar{1}3:xx}^P(O) = -626.0$ ppm; $\sigma_{12\bar{1}3:yy}^P(O) = -31.5$ ppm) transitions predominantly contribute to $\sigma^P(O)$; additionally, the
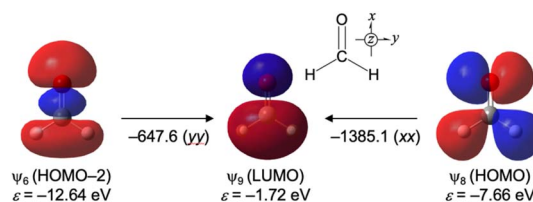

Fig. 11 Main contributions from each $\psi_i \rightarrow \psi_a$ transition to the components of $\sigma^P(O)$ in $H_2C=O$ (**34**), together with the axes.

Table 15 The $\sigma^d(O)$, $\sigma^P(O)$ and $\sigma^t(O)$ values of $H(HO)C=O$ (C_s), given separately by each $\psi_i{}^a$

MO (i in ψ_i)	$\sigma_i^d(O)$	$\sigma_i^P(O)$	$\sigma_i^t(O)$
H(HO)C=O* (35: C_s)			
1,3	0.01	0.00	0.01
2	270.61	0.00	270.61
4	9.56	−6.12	3.44
5	23.30	−21.95	1.35
6	4.29	3.74	8.03
7	7.16	15.69	22.85
8	12.87	−83.26	−70.39
9	12.53	−10.06	2.47
10	15.65	−130.36	−114.71
11	18.37	−18.43	−0.07
12	30.15	−234.06	−203.91
ψ_{occ} to ψ_{occ}		−21.96	
Total	404.48	−506.77	−102.29
H(HO*)C=O (36: C_s)			
1	270.61	0.00	270.61
2,3	0.02	0.02	0.04
4	22.33	−10.63	11.70
5	13.44	−6.15	7.29
6	15.46	−10.24	5.23
7	11.01	−40.96	−29.95
8	10.18	−8.84	1.35
9	17.85	−33.89	−16.04
10	9.22	−120.24	−111.02
11	18.74	−29.95	−11.22
12	10.95	−42.16	−31.21
ψ_{occ} to ψ_{occ}		18.67	
Total	399.81	−284.37	115.44

^{a} Using the GIAO method under B3LYP/BSS-A.

$\psi_{10} \to \psi_{13}$ ($\sigma^{P}_{10\bar{1}3:yy}(O) = -198.3$ ppm; $\sigma^{P}_{10\bar{1}3:xx}(O) = -53.0$ ppm) transition predominantly contributes to $\sigma^{P}(O)$ of H(HO*)C=O.

Fig. 12a and b illustrate the selected $\psi_i \to \psi_a$ transitions in H(HO)C=O* and H(HO*)C=O, respectively, along with the molecular axes. While ψ_{10} and ψ_{12}, in the $\psi_{10} \to \psi_{13}$ and $\psi_{12} \to \psi_{13}$ transitions of H(HO)C=O*, have the main character of occupied $\sigma(C=O)$ and $n_p(O)$, respectively, ψ_{13} has the vacant $\pi^*(C=O)$ character. Therefore, ψ_{10} ($\sigma(C=O)$) and ψ_{12} ($n_p(O)$) act as excellent donors, while ψ_{13} ($\pi^*(C=O)$) operates as an excellent acceptor in H(HO)C=O*. However, ψ_{11} ($\pi(C=O)$) seems not a good donor in the transitions, again, if compared with ψ_{10} and ψ_{12}. Similarly, ψ_{10} and ψ_{13}, in the $\psi_{10} \to \psi_{13}$ transition of H(HO*)C=O, have the main character of the occupied $\sigma(C=O)$ and the vacant $\pi^*(C=O)$, respectively. Thus, ψ_{10} ($\sigma(C=O)$) acts as a good donor and ψ_{13} ($\pi^*(C=O)$) operates as a good acceptor in the transitions to produce (large) $\sigma^{P}(O)$ of H(HO*)C=O.

The ($\Delta\sigma^{d}(O)_e$, $\Delta\sigma^{P}(O)_e$, $\Delta\sigma^{t}(O)_e$) values for the process from $H_2C=O$ to H(HO)C=O* are also of interest. The values are (0.0, 327.0, 327.0 ppm), which means that the H(HO)C=O* signal will appear at much higher field of 327.0 ppm from that of $H_2C=O^*$.

The specific π-type O–C=O interaction is responsible for the results. The charge on H(HO)C=O* is less positive than that on $H_2C=O$, due to the donation from HO to C=O in H(HO)C=O, which leads to the upfield shift. The wider extension of the MOs over the entire molecule in H(HO)C=O needs to be considered, again, although it would be complex. The smaller occupancy of an important orbital in H(HO)C=O*, relative to that in $H_2C=O^*$, would not effectively operate to produce a larger $\sigma^{P}(O)$ in magnitude. The energy differences in the transitions also affect on $\sigma^{P}(O)$, along with the charge on O. A more upfield $\sigma^{P}(O)$ shift is predicted if the charge on O becomes less positive, although the energy term would show the inverse direction from the factor of the charge.

The much larger downfield shift for $H_2C=O$ relative to H(HO)C=O* is effectively reproduced in the calculations. The large upfield shifts in RC(=O)NHR' and ROC(=O)OR', relative to $H_2C=O$, can also be understood based on the structural
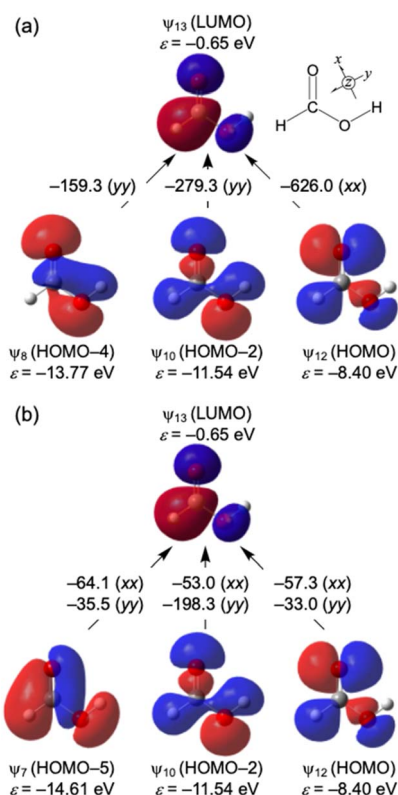

Fig. 12 Main contributions from each $\psi_i \to \psi_a$ transition to the components of $\sigma^{P}(O)$ in H(HO)C=O* (35) (a) and H(HO*)C=O (36) (b), together with the axes.

similarities to H(HO)C=O, relative to $H_2C=O$. Specifically, the analysis of $H_2C=O$ and H(HO)C=O can aid in the understanding of the ^{17}O NMR chemical shifts of similar structures. However, further investigations are needed to understand the much higher downfield shifts of the nitroso species and ozone.

Visualization of $\Delta\sigma^{d}(O)$, $\Delta\sigma^{P}(O)$ and $\Delta\sigma^{t}(O)$ in some oxygen containing species

The $\Delta\sigma^{d}(O)$, $\Delta\sigma^{P}(O)$ ($=\sigma^{P}(O)$), $\Delta\sigma^{t}(O)$ values and the components are plotted for Me_2O, Et_2O, $H_2C=CHOH$, H(HO)C=O* and H(HO*)C=O. Fig. 13 shows the plot. The contributions from the occupied-to-occupied orbital ($\psi_i \to \psi_j$) transitions, shown in green in Fig. 13, are all positive, except for H(HO)C=O*. The $\sigma^{P}(O)$ values are all negative, of which magnitude is small for Me_2O but very large for H(HO)C=O*. The contributions from the $\psi_i \to \psi_j$ transitions seem to decrease as the magnitudes of $\sigma^{P}(O)$ increase. MOs, mainly constructed by the $2p_x(O)$, $2p_y(O)$ and $2p_z(O)$ AOs, should contribute much on $\sigma^{P}(O)$. The contributions to $\sigma^{P}(O)$ are well visualized, which helps us to understand the rule and the mechanism of $\sigma^*(O: * = d, p$ and $t)$.

Contributions from occupied-to-occupied orbital transitions to $\sigma^{P}(O)$

The occupied-to-occupied orbital ($\psi_i \to \psi_j$) transitions are usually not considered to be important; therefore, they are often neglected in the discussion. However, they contribute to $\sigma^{P}(O)$

Table 16 Main contributions from occupied to unoccupied orbital transitions on $\sigma^{P}(O)$ of H(HO)C=O (C_s)[a]

$i \to a$[b]	$\sigma^{P}_{i \to a:xx}(O)$	$\sigma^{P}_{i \to a:yy}(O)$	$\sigma^{P}_{i \to a:zz}(O)$	$\sigma^{P}_{i \to a}(O)$
H(HO)C=O* (35)				
$5 \to 13$	0.56	−30.94	0.00	−10.13
$7 \to 13$	85.27	−2.96	0.00	27.44
$8 \to 13$	−0.68	−159.30	0.00	−53.33
$10 \to 13$	−45.89	−279.32	0.00	−108.40
$12 \to 13$	−625.99	−31.46	0.00	−219.15
H(HO*)C=O (36)				
$7 \to 13$	−64.11	−35.48	0.00	−33.20
$8 \to 13$	2.20	70.95	0.00	24.38
$10 \to 13$	−53.03	−198.27	0.00	−83.77
$10 \to 20$	0.00	0.00	−45.92	−15.31
$12 \to 13$	−57.30	−32.99	0.00	−30.10

[a] Calculated with the GIAO method under B3LYP/BSS-A. The magnitudes of $\sigma^{P}_{i \to a}(O)$ larger than 10 ppm are shown. [b] In $\psi_i \to \psi_a$.

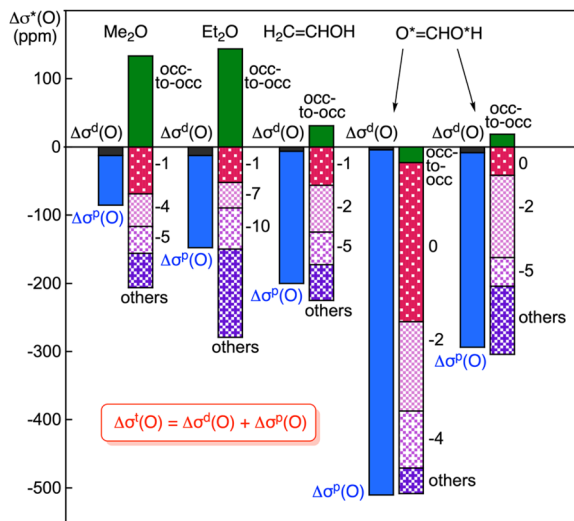**Fig. 13** Plots of $\Delta\sigma^d(O)$, $\Delta\sigma^p(O)$ ($=\sigma^p(O)$), $\Delta\sigma^t(O)$ and the components, for Me$_2$O, Et$_2$O, H$_2$C=CHOH, H(HO)C=O* and H(HO*)C=O. Each MO contributing to $\sigma^p(O)$ is shown by -n in HOMO-n.

Table 17 The contributions from the occupied-to-occupied orbital ($\psi_i \rightarrow \psi_j$) transitions to $\sigma^p(O)$ in some oxygen containing species[a]

Species	$\sigma^p(O)_{o-o}$	Species	$\sigma^p(O)_{o-o}$
HO$^-$ (**2**: $C_{\infty v}$)	114.41	H$_2$C=CHOH (**31**: C_s)	31.50
H$_2$O (**7**: C_{2v})	109.30	H$_2$C=O (**34**: C_{2v})	−39.79
H$_3$O$^+$ (**25**: C_{3v})	57.17	H(HO)C=O* (**35**: C_s)	−21.96
Me$_2$O (**14**: C_{2v})	133.50	H(HO*)C=O (**36**: C_s)	18.67
Et$_2$O (**20**: C_{2v})	142.90		

[a] Using the GIAO method under B3LYP/BSS-A.

more than expected, in some cases. Such transitions should arise through the redistribution of electrons in a species under an applied magnetic field. Table 17 summarizes the values, again, which are shown in some Tables in the text.

The paramagnetic contributions from the occupied-to-occupied transitions, $\sigma^p(O)_{o-o}$, are larger than 100 ppm for HO$^-$ ($C_{\infty v}$), H$_2$O (C_{2v}), Me$_2$O (C_{2v}) and Et$_2$O ($C_{\infty v}$), which form group **A** (g(**A**)). The $\sigma^p(O)_{o-o}$ values are less than 60 ppm for H$_2$C=CHOH (C_s), H$_2$C=O (C_{2v}), H(HO)C=O* (C_s), H(HO*)C=O (C_s) and H$_3$O$^+$ (C_{3v}), which belong to g(**B**). According to the discussion about the data in Fig. 13, $\sigma^p(O)_{o-o}$ are plotted *versus* $\sigma^p(O)$, to examine the relationship between the two. The plot is shown in Fig. S11 of the ESI.† While the correlation was poor for g(**A**) ($y = 105.70-0.261x$: $R_c^2 = 0.625$), whereas a very good correlation was obtained for g(**B**), if analysed with a quadric function ($y = 82.87 + 0.288x + 0.00017x^2$: $R_c^2 = 0.996$). Indeed $\sigma^p(O)_{o-o}$ will change depending on $\sigma^p(O)$, but the behaviour seems complex.

Conclusions

The ^{1}H NMR chemical shifts are controlled predominantly by the σ^d term; therefore, $\delta(^1$H) are explained mainly by Q(H), especially for saturated organic species, although other terms,

such as the aromatic ring current effect, become important in some cases. For the atoms of the third and higher periods, the spectra can be analysed based on the σ^p term, predominantly, neglecting the σ^d term as the relative values. In the case of the atoms of the second period, the NMR chemical shifts are controlled by both σ^d and σ^p terms, where the contribution ratios will change depending on the atoms and the species containing the atoms. Namely, the analysis of the spectra for the atoms of the second period will be essentially more complex relative to other cases. NMR spectra, containing $\delta(^{17}$O), are usually analysed with the guidance of empirical rules. Indeed, the empirical rules are useful for assigning the spectra, but the origins of chemical shifts are difficult to understand based on such rules. Then, our research interested is to establish the plain rules founded in theory with the origin of the ^{17}O NMR chemical shifts for the better understanding of the phenomena, which is the aim of this study. The origin should be visualized based on the specific concepts, such as molecular orbitals. This purpose is given more importance than the usual one in NMR calculations to reproduce the observed values accurately and/or to predict well the shift values of unknown target compounds.

NMR chemical shifts of ^{17}O are analysed employing the calculated σ^d, σ^p and σ^t terms. The contributions from $\sigma^d(O)$ to $\sigma^t(O)$ are approximately one tenth of those from $\sigma^p(O)$, although the ratio changes depending on the oxygen containing species. The plots of $\sigma^d(O)$ *versus* Q(O) for O^x ($x = -2$, 0, 2, 4 and 6) effectively follow a quadratic regression curve, and those for H$_2$O, HO$^+$, HO$^-$, and H$_3$O$^+$ are located (very) near the curve. Therefore, the $\sigma^d(O)$ values can be understood based on Q(O) for the species. However, $\sigma^d(O)$ values of ROH and ROR' (R, R': alkyl group) change depending on R and R' but not on Q(O). The σ^p values were analysed based on the occupied-to-unoccupied orbital ($\psi_i \rightarrow \psi_a$) transitions, which arose $\sigma^p(O)$. The relationship between $\sigma^p(O)$ and Q(O) was not examined, which would be hidden in the complex combinations of in the $\psi_i \rightarrow \psi_a$ transitions, as shown in eqn (6). Specifically, a broad (but not so strong) relationship between δ(O) and Q(O) has been reported, as expected, if the conditions are satisfied; however, an explicit relationship is not observed for most cases. The occupied-to-occupied orbital ($\psi_i \rightarrow \psi_j$) transitions are also examined, of which contributions to $\sigma^p(O)$ are denoted by $\sigma^p(O)_{o-o}$. The good proportionality between $\sigma^p(O)_{o-o}$ and $\sigma^p(O)$ was confirmed in some cases, but not widely. The treatments provided useful information for $\sigma^p(O)$, where the contributions from the $\psi_i \rightarrow \psi_j$ transitions are usually neglected. The relationships between Q(O) and between $\sigma^p(O)$ and the orbital–orbital transitions (interactions) are widely clarified, in this work.

The origin of the effects is visualized based on the occupied-to-unoccupied orbital ($\psi_i \rightarrow \psi_a$) transitions, where $\sigma^p(O)$ arises from the transitions. As a result, the plain rules with the origin can be more easily imaged and understood through the contributions of transitions to the effects also by the experimental scientists, including the authors. The results will help to understand the role of O in the specific position of a compound in question and the mechanisms to arise the shift values. This work also has the potential to provide an understanding of the δ(O) values of unknown species and facilitate new concepts for the strategies to

create highly functional materials based the observed $\delta(O)$ values, along with the calculated $\sigma^d(O)$ and $\sigma^p(O)$ values.

Author contributions

W. N. and S. H. formulated the project. K. M. contributed to investigation and writing. W. N. and S. H. organized the data, contributed to supervision, data curation, resources and writing – review & editing the paper. All authors have read and agreed to the published version of the manuscript.

Conflicts of interest

The authors declare no conflicts of interest.

Acknowledgements

Notes and references

1 *Encyclopedia of Nuclear Magnetic Resonance*, ed. D. M. Grant and R. K. Harris, John Wiley & Sons, New York, 1996.

2 *Encyclopedia of Nuclear Magnetic Resonance*, ed. R. K. Harris and R. E. Wasylishen, John Wiley & Sons, New York, 2012.

3 *Nuclear Magnetic Shieldings and Molecular Structure*, ed. J. A. Tossell, Kluwer Academic Publishers, Dordrecht, Boston, London, 1993.

4 *Calculation of NMR and EPR Parameters; Theory and Applications*, ed. M. Kaupp, M. Bühl and V. G. Malkin, Wiley-VCH Verlag GmbH & Co. KGaA, Weinheim, 2004.

5 C. Geletneky and S. Berger, *Eur. J. Org Chem.*, 1998, 1625–1627.

6 F. Mocci, G. Uccheddu, A. Frongia and G. Cerioni, *J. Org. Chem.*, 2007, **72**, 4163–4168.

7 I. P. Gerothanassis, *Prog. Nucl. Magn. Reson. Spectrosc.*, 2010, **56**, 95–197.

8 I. P. Gerothanassis, *Prog. Nucl. Magn. Reson. Spectrosc.*, 2010, **57**, 1–110.

9 L. B. Krivdin, *Magn. Reson. Spectrosc.*, 2023, **61**, 507–529.

10 W. Saenger, *Principles of Nucleic Acid Structures*, Springer, Berlin, 1984.

11 X. Wang, A. R. Chandrasekaran, Z. Shen, Y. P. Ohayon, T. Wang, M. E. Kizer, R. Sha, C. Mao, H. Yan, X. Zhang, S. Liao, B. Ding, B. Chakraborty, N. Jonoska, D. Niu, H. Gu, J. Chao, X. Gao, Y. Li, T. Ciengshin and N. C. Seeman, *Chem. Rev.*, 2019, **119**, 6273–6289.

12 J.-L. Mergny and D. Sen, *Chem. Rev.*, 2019, **119**, 6290–6325.

13 F. C. Simmel, B. Yurke and H. R. Singh, *Chem. Rev.*, 2019, **119**, 6326–6369.

14 S. S. Wang and A. D. Ellington, *Chem. Rev.*, 2019, **119**, 6370–6383.

15 M. Madsen and K. V. Gothelf, *Chem. Rev.*, 2019, **119**, 6384–6458.

16 S. Muniyappan, Y. Lin, Y.-H. Lee and J. H. Kim, *Biology*, 2021, **10**, 453–461.

17 B. Lin, I. Hung, Z. Gan, P.-H. Chien, H. L. Spencer, S. P. Smith and G. Wu, *ChemBioChem*, 2021, **22**, 826–829.

18 V. Balevičius, K. Aidas, A. Maršalka, F. Kuliešius, V. Jakubkienė and S. Tumkevičius, *Lith. J. Phys.*, 2022, **62**, 114–125.

19 W. Nakanishi, S. Hayashi and M. Hada, *Chem.–Eur. J.*, 2007, **13**, 5282–5293.

20 K. Kanda, H. Nakatsuji and T. Yonezawa, *J. Am. Chem. Soc.*, 1984, **106**, 5888–5892.

21 *Molecular Quantum Mechanics*, ed. P. W. Atkins and R. S. Friedman, Oxford: New York, 3rd edn, 1997, ch. 13.

22 Indeed, this decomposition includes small arbitrariness due to the coordinate origin dependence, but it does not damage our insights into the ^{17}O NMR spectroscopy.

23 The occupied-to-unoccupied orbital $(\psi_i \rightarrow \psi_a)$ transitions mainly contribute to σ^p, whereas the occupied-to-occupied orbital $(\psi_i \rightarrow \psi_j)$ transitions sometimes play an important role in σ^p.

24 Based on the second-order perturbation theory at the level of the HF and single-excitation CI approximation, $\sigma^p_{i \rightarrow a}$ on a resonance nucleus N is shown to be proportional to reciprocal orbital energy gap $(\varepsilon_a - \varepsilon_i)^{-1}$ as expressed in eqn (5), where ψ_k is the k-th orbital function, $\hat{L}_{z,N}$ is orbital angular momentum around the resonance nucleus, and r_N is the distance from the nucleus N.

25 M. J. Frisch, G. W. Trucks, H. B. Schlegel, G. E. Scuseria, M. A. Robb, J. R. Cheeseman, G. Scalmani, V. Barone, B. Mennucci, G. A. Petersson, H. Nakatsuji, M. Caricato, X. Li, H. P. Hratchian, A. F. Izmaylov, J. Bloino, G. Zheng, J. L. Sonnenberg, M. Hada, M. Ehara, K. Toyota, R. Fukuda, J. Hasegawa, M. Ishida, T. Nakajima, Y. Honda, O. Kitao, H. Nakai, T. Vreven, J. A. Montgomery Jr, J. E. Peralta, F. Ogliaro, M. Bearpark, J. J. Heyd, E. Brothers, K. N. Kudin, V. N. Staroverov, R. Kobayashi, J. Normand, K. Raghavachari, A. Rendell, J. C. Burant, S. S. Iyengar, J. Tomasi, M. Cossi, N. Rega, J. M. Millam, M. Klene, J. E. Knox, J. B. Cross, V. Bakken, C. Adamo, J. Jaramillo, R. Gomperts, R. E. Stratmann, O. Yazyev, A. J. Austin, R. Cammi, C. Pomelli, J. W. Ochterski, R. L. Martin, K. Morokuma, V. G. Zakrzewski, G. A. Voth, P. Salvador, J. J. Dannenberg, S. Dapprich, A. D. Daniels, Ö. Farkas, J. B. Foresman, J. V. Ortiz, J. Cioslowski and D. J. Fox, *Gaussian 09, Revision D.01*, Gaussian, Inc., Wallingford CT, 2009.

26 A. D. Becke, *Phys. Rev.*, 1988, **38**, 3098–3100.

27 A. D. Becke, *J. Chem. Phys.*, 1993, **98**, 5648–5652.

28 C. Lee, W. Yang and R. G. Parr, *Phys. Rev. B: Condens. Matter Mater. Phys.*, 1988, **37**, 785–789.

29 B. Miehlich, A. Savin, H. Stall and H. Preuss, *Chem. Phys. Lett.*, 1989, **157**, 200–206.

30 C. Møller and M. S. Plesset, *Phys. Rev.*, 1934, **46**, 618–622.

31 J. Gauss, *J. Chem. Phys.*, 1993, **99**, 3629–3643.

32 J. Gauss and B. Bunsenges, *Phys. Chem.*, 1995, **99**, 1001–1008.

33 K. Wolinski, J. F. Hinton and P. Pulay, *J. Am. Chem. Soc.*, 1990, **112**, 8251–8260.

34 K. Wolinski and A. Sadlej, *Mol. Phys.*, 1980, **41**, 1419–1430.

35 R. Ditchfield, *Mol. Phys.*, 1974, **27**, 789–807.

36 R. McWeeny, *Phys. Rev.*, 1962, **126**, 1028–1034.

37 F. London, *J. Phys. Radium*, 1937, **8**, 397–409.

38 T. Yanai, D. P. Tew and N. C. A. Handy, *Chem. Phys. Lett.*, 2004, **393**, 51–57.

39 J. P. Perdew, K. Burke and M. Ernzerhof, *Phys. Rev. Lett.*, 1996, **77**, 3865–3868.

40 C. Adamo and V. Barone, *J. Chem. Phys.*, 1999, **110**, 6158–6169.

41 T. M. Henderson, A. F. Izmaylov, G. Scalmani and G. E. Scuseria, *J. Chem. Phys.*, 2009, **131**, 044108.

42 J.-D. Chai and M. Head-Gordon, *Phys. Chem. Chem. Phys.*, 2008, **10**, 6615–6620.

43 F. Weigend and R. Ahlrichs, *Phys. Chem. Chem. Phys.*, 2005, **7**, 3297–3305.

44 F. Weigend and R. Ahlrichs, *Phys. Chem. Chem. Phys.*, 2006, **8**, 1057–1065.

45 J. Tomasi, B. Mennucci and R. Cammi, *Chem. Rev.*, 2005, **105**, 2999–3093.

46 The utility program was provided by Prof. Hada and Dr Yamaki of Tokyo Metropolitan University. It is derived from the NMR program in the Gaussian program, which made some processes, necessary for our discussion, possible to be printed out, such as the contributions from the occupied orbitals and/or the orbital-to-orbital transitions[51]

47 E. D. Glendening, J. K. Badenhoop, A. E. Reed, J. E. Carpenter, J. A. Bohmann, C. M. Morales, C. R. Landis and F. Weinhold, *NBO Version 6.0*, 2013.

48 R. A. Klein, B. Mennucci and J. Tomasi, *J. Phys. Chem. A*, 2004, **108**, 5851–5863.

49 E. Taskinen, *Magn. Reson. Chem.*, 1998, **36**, 573–578.

50 J.-C. Zhuo, *Molecules*, 1999, **4**, 320–328.

51 Essentially the same analysis can be achieved by using the ADF program. The ADF program should be explained here.